

The Propagation Group

Indoor/Outdoor Location of Cellular Handsets Based on Received Signal Strength


Document ID: PG-TR-040618-JZ

Date: June 18, 2004

Jian Zhu and Prof. Gregory D. Durgin
777 Atlantic Ave. Atlanta, GA 30332-0250
E-mail: durgin@ece.gatech.edu
Voice: (404)894-8169 Fax: (404)894-5935
<http://users.ece.gatech.edu/~durgin>

No portion of this document may be copied or reproduced without written (e-mail) consent of the Georgia Institute of Technology.

CONTENTS

LIST OF FIGURES	x
LIST OF TABLES	xii
1 INTRODUCTION	1
1.1 Overview	1
1.2 Current Cellular Location Technology	5
1.3 How RSSI-based Radiolocation Works	7
1.4 Key Outcomes	9
2 MEASUREMENT PLAN	10
2.1 Setup Overview	11
2.2 Equipment and Calibration	13
2.2.1 Comarco LT200 Unit	13
2.2.2 Ericsson TEMS Light 3.0 Unit	14
2.2.3 Calibration Procedure	14
3 DATA COLLECTION	20
3.1 Building Construction	20
3.1.1 Architecture (West)	22
3.1.2 Architecture (East)	23
3.1.3 Van Leer (ECE)	23
3.1.4 Pettit MiRC	25
3.1.5 College of Computing (CoC)	26
 Propagation Group <small>Georgia Institute of Technology</small>	vii

3.1.6	Cherry Emerson	28
3.1.7	Howey Physics	29
3.1.8	Mason (Civil Engineering)	30
3.1.9	Bunger-Henry	33
3.1.10	Student Center Parking Deck	33
3.2	Outdoor Measurements	36
3.2.1	Drive Test Measurement	36
3.2.2	Walking Outdoor Measurement	37
3.3	Indoor Measurements	38
3.4	GIS Data	44
4	DATA ANALYSIS	46
4.1	Angle-Related Penetration Loss	46
4.1.1	Basics of Indoor Propagation	46
4.1.2	Indoor Propagation Issues for RSS Location	47
4.1.3	Octant Model of Orientation Loss	48
4.1.4	Octant Penetration Values	51
4.1.5	Building Sample Analysis	51
4.2	Handset RSS Distribution	52
4.2.1	Indoor RSS Distribution	53
4.2.2	Outdoor RSS Distribution	54
4.2.3	Indoor/Outdoor Comparison	54
5	PREPARING RF MAPS	57
5.1	Introduction	57
5.2	Simple Propagation Modeling	57
5.3	Interpolating Measurements into RF Maps	59
5.4	Three Types of Databases	61
5.4.1	Outdoor Measurements (Level 1)	61
5.4.2	Outdoor Measurements and Indoor Modeling (Level 2)	62
5.4.3	Outdoor and Indoor Measurements (Level 3)	64
6	LOCATION PERFORMANCE	66
6.1	Overview of Location Algorithm	66

6.1.1	Definition of M-Distance—Euclidean Distance	66
6.1.2	Metric of Location Performance	67
6.1.3	Dart-Throwing Probability	68
6.2	Performance	70
6.2.1	Absolute RSS Location	70
6.2.2	Relative RSSI Location	71
6.2.3	Hybrid-Method RSS Location	73
6.2.4	Hybrid-Method RSS Location with Averaging	76
6.2.5	Hybrid-Method RSSI Location for only 6 Sectors	78
6.2.6	Pure Outdoor Location Performance	78
7	CONCLUSIONS	82
8	ACKNOWLEDGEMENT	84
	BIBLIOGRAPHY	85

List of Figures

1.1	The Predicted Signal Data (PSD) stores a raster database of all RSSI from audible base stations within the network.	7
2.1	Indoor/Outdoor “location laboratory” at Georgia Tech campus in semi-urban Atlanta, GA.	11
2.2	Scanner setup illustration (Comarco LT200 Users Guide[pg162]).	13
2.3	Actual SComarco canner Setup.	15
2.4	Actual TEMS unit Setup.	16
2.5	Rooftop Calibration Route.	17
3.1	South side of Architecture (West).	23
3.2	North side of Architecture (East).	24
3.3	South side of Van Leer (ECE).	26
3.4	West side of Pettit (MiRC).	27
3.5	West side of College of Computing (CoC).	28
3.6	Northwest side of College of Computing (CoC).	29
3.7	West side of Cherry Emerson.	30
3.8	North side of Howey Physics.	31
3.9	North side of Mason (Civil Engineering)).	32
3.10	East side of Bunger-Henry.	34
3.11	East side of Student Center Parking Deck (medium-tier base station on utility pole on the corner of the structure.)	35
3.12	Driving route for outdoor drive-test measurement.	37
3.13	Georgia Tech student researcher Chris Durkin takes an outdoor walking measurement outside Bunger-Henry.	38

3.14	Georgia Tech student researcher Alenka Zajic takes an outdoor walking measurement outside student center parking deck.	39
3.15	Georgia Tech student researcher Joshua Griffin takes an indoor walking measurement inside Howey physics.	40
3.16	Georgia Tech student researcher Albert Lu takes an indoor walking measurement inside Architecture (East).	41
3.17	Georgia Tech student researcher Jian Zhu takes an handset walking measurement inside Van Leer.	42
3.18	Indoor / outdoor measurement procedure measurement route.	42
3.19	Measurement Route Record at Architecture Building.	43
3.20	Binary building footprint inside experiment area.	45
4.1	Directions are broken into uniform angle ranges called <i>octants</i> . The thick line is the building surface. Above is outdoors, below is indoors.	50
4.2	RSS at Architecture Building.	52
4.3	Indoor Received Signal Strength Aggregate (RSSA) distribution measured at Georgia Tech campus.	54
4.4	Outdoor Received Signal Strength Aggregate (RSSA) distribution measured at Georgia Tech campus.	55
4.5	Indoor and outdoor RSSA theoretical distribution.	56
5.1	RF map based on pure prediction using a modified Hata model.	59
5.2	Marked raster regions (in gray) for (a) a single measurement and (b) a path of measurements.	60
5.3	RF map calibrated with outdoor drive test measurements for use in a Level 1 PSD. (Map units in dBm.)	62
5.4	RF map calibrated with outdoor drive test measurements and indoor modeling for use in a Level 2 PSD. (Map units in dBm.)	63
5.5	RF map calibrated with outdoor and indoor measurements for use in a Level 3 PSD. (Map units in dBm.)	65
6.1	Calculation the probability of indoor call or outdoor call from RSSA	74

List of Tables

2.1	Measurement data of DCCH 797 from CoC base station.	19
3.1	Building construction summary for Georgia Tech.	21
3.2	Building Construction of Architecture (West).	22
3.3	Building Construction of Architecture (East).	24
3.4	Building Construction of Van Leer (ECE).	25
3.5	Building Construction of Pettit (MiRC).	27
3.6	Building Construction of College of Computing (CoC).	28
3.7	Building Construction of Cherry Emerson.	30
3.8	Building Construction of Howey Physics.	31
3.9	Building Construction of Mason (Civil Engineering).	32
3.10	Building Construction of Bunger-Henry.	33
3.11	Building Construction of Student Center Parking Deck	34
4.1	Octant penetration values.	51
6.1	Discrimination rate of the absolute RSS location algorithm. (Dart-throwing probability of 34%.)	71
6.2	Location error statistics of absolute RSS location algorithm.	71
6.3	Discrimination rate of relative RSS location algorithm. (Dart-throwing probability is 34%)	73
6.4	Location Error Statistics of Relative RSS location algorithm	73
6.5	Discrimination rate of Hybrid-Method RSS location algorithm. (Dart-throwing probability is 34%.)	76
6.6	Location error statistics of Hybrid-Method RSS location algorithm	76

6.7	Discrimination rate of Hybrid-Method RSS location algorithm. (Linear averaging of 10 NMRs, dart-throwing probability of 34%.)	77
6.8	Location Error Statistics of Hybrid-Method RSS location algorithm. Linear averaging of 10 NMRs.	77
6.9	Discrimination rate of Hybrid-Method RSS location algorithm. (Single NMR, 6 sectors, dart-throwing probability of 34%.)	79
6.10	Location error statistics of Hybrid-Method RSS location algorithm. (Single NMR, 6 sectors)	79
6.11	Discrimination rate of Hybrid-Method RSS location algorithm with averaging. (Linear averaging of 10 NMRs, 6 sectors, dart-throwing probability of 34%.)	80
6.12	Location error statistics of Hybrid-Method RSS location algorithm with averaging. (Linear averaging of 10 NMRs, 6 sectors.)	80
6.13	Discrimination rate of Hybrid-Method RSS location algorithm.	80
6.14	Location error statistics of Hybrid-Method RSS location algorithm.	81

INTRODUCTION

1.1 Overview

This report documents the results of a ground-breaking set of experiments for mobile handset location within the commercial cellular telephone network. With particular emphasis on the US emergency 911 (E911) location problem, we demonstrate the viability of Received Signal Strength (RSS) techniques to meet the safety requirements set forth by the Federal Communications Commission (FCC) in a semi-urban environment. Furthermore, we conclusively show that RSS location techniques are also accurate for indoor users – a characteristic unique among all currently proposed E911 technologies. Our measurement campaign and test results indicate RSS-based techniques can approach or even surpass the FCC guidelines of 100m accuracy 67% of the time and 300m accuracy 95% for a network with a majority of indoor users. Since most cellular phone calls are now placed from indoor environments, this result has enormous implications for the E911 rollout and public safety.

The RSS location technique is a relatively new and controversial method for radiolocation within the cellular network. The principle idea is to solve for users' xy -coordinates by studying signal strength measurements of nearby cellular sectors made by their handsets. All digital handsets measure the signal strength of neighboring control channels, and report the results back to the serving base station in

the form of a *network measurement report* (NMR). All digital cellular air interfaces include the ability to report NMRs, largely for the purpose of performing *mobile-assisted hand-offs* (MAHOs). Once this NMR has been received at the base station and routed to the central switching office, its set of signal powers is matched to those in a well-calibrated database of RF maps. The closest match between measured and predicted signals likely occurs at a point near the groundtruth location within the database. This technique is similar to the scheme used to locate WLAN modems in a much smaller-scale location problem [Che02]. The technique has been proposed for use in the cellular network by [Wei03].

To perform this study in radiolocation, we turned the Georgia Tech campus into the world's first indoor/outdoor cellular location laboratory. The ensuing location tests were performed on an 850 MHz IS-136 cellular network in mid-town Atlanta. The Georgia Tech campus approximates a typical semi-urban or dense suburban area with streets, moderate green space, and many 4-5 story academic and office buildings. Although the potential population density of cellular users is high, there are no skyscrapers or canyons that would be associated with dense urban deployments. A database of RF coverage maps for all nearby serving sectors was created from a combination of propagation modeling and varying degrees of indoor and outdoor measurement calibration using a Comarco IS136 scanner with baseband decoding. Real, pedestrian-style handset measurements were taken with an Ericsson handset connected to an Ericsson TEMs data collection unit.

The results in this study show that RSS location techniques can satisfy the FCC E911 requirements for outdoor handsets in semi-urban environments. This result is shown in Section 6.2.6. When a majority of the test handset data originates from indoor locations (as it would in real life), the performance degrades somewhat. For example, the error distance between a location estimate and a handset's groundtruth

position drops from 100m or less 66% of the time to 100m or less 56% of the time (see the indoor analysis in Section 6.2.3). However, this report demonstrates a variety of ways to recover the lost accuracy by modifying the location algorithms, adding indoor calibration measurements, modeling indoor propagation using satellite photogrammetry, and using sequential handset measurements. The most accurate location algorithm is documented in Section 6.2.4; using a sequence of 10 linearly-averaged handset measurements and RF maps calibrated with both outdoor and indoor measurements, the error distance for this case is 100m or less 78% of the time and 300m or less 98% of the time. This upper limit of performance is *well* above the FCC E911 requirements.

This measurement campaign lasted for 4 months (January through April) in the beginning of 2004. All data points were tagged with absolute longitude and latitude coordinates taken from a Global Positioning System (GPS) radio; however, due to the limitations of GPS, many outdoor coordinates and all indoor coordinates had to be painstakingly estimated from geo-referenced maps of campus and manually entered into the database. This is one source of error in our measurements. There are other unique sources of error in our measurements that may make our results somewhat pessimistic. For example, there was a seasonal change in the middle of our data collections where leaves grew back on the campus trees, changing the propagation characteristics by several dB. Also, one of the large buildings within our test area was demolished in the middle of our campaign. We also used a fairly simple location algorithm since we were concentrating on the more complicated question of indoor feasibility. There are many other algorithms that have been proposed which could improve the performance [Aso00][Lai01][PB00].

Several recommendations emerge from this study. Our experimental results suggest that RSS-based techniques may be resilient enough for deployment as a stand-alone position location technology for satisfying the FCC's E911 requirements in most

populated areas. There are still several questions about this technology that need to be addressed. First and foremost, it is unclear how much cost and effort that is required to *maintain* the performance in cellular networks that, to one degree or another, are always undergoing buildout, optimization, or modification.

Ultimately the ideal solution for the US E911 problem will be a hybrid combination of handset-based Global Positioning System (GPS) technology and an RSS-based location system. These two technologies seem to complement each other so well. GPS works in rural, open-sky environments where all network-based location solution tends to degrade due to the low density of base stations. Conversely, GPS fails whenever satellite links become obstructed. This can happen in any environment, but is particularly acute in urban and indoor areas – precisely the places that RSS radiolocation works best. If public safety is the primary concern, then this long-term tandem of location technologies seems to be most sensible.

At Georgia Tech, we are continuing to pursue research in the field of RSS-based position location. Several areas of proposed research are:

- How well do RSS-based location technologies perform in a wide variety of in-building environments (residences, skyscrapers, retail establishments, etc.)?
- How do we improve state-of-the-art propagation modeling to build accurate RSS databases in regions devoid of measurement calibration?
- How can the RSS databases be efficiently calibrated and maintained?

There is much work left to be done in development of this late-coming location technology, but initial results are quite promising.

1.2 Current Cellular Location Technology

Position location in the cellular network is not a new problem [Kos00], [Chr00]. There have been a number of proposed solutions[Zha02] which include angle-of-arrival (AOA)[Sak92], [Klu98], time-of-arrival (TOA)[Caf98], [Caf00], time difference of arrival (TDOA), enhanced observed time difference (EOTD), assisted global position system (AGPS), and received signal-strength signatures (RSSS)[Wei03], [Aso01], [Che02].

Various wireless location techniques can be classified into four categories:

- 1) angle-based location, (i.e. AOA)
- 2) time-based location, (i.e. TOA, TDOA, EOTD)
- 3) GPS system based location (i.e. GPS, AGPS), and
- 4) received signal-strength (RSS) Location.

Angle-based location uses the precise measurement of the direction along the line of maximum signal strength at two or more base stations to triangulate the location of a handset. These techniques require high signal fidelity for superresolution array processing. Therefore, sophisticated and expensive antenna array hardware is required for each base station.

Time-based solutions measure either the absolute or relative arrival times of several signals, backsolving the location of a handset through triangulation. Time-based solutions require precise synchronization for all base station clocks. Both TDMA and GSM (the most largely deployed wireless system in the world) do not include precise time synchronization of measurement in their original air interface standards. Thus, additional equipment is also required for each base station. Because of the new hardware requirements, the deployment of time-based and angle-based schemes would cost several million dollars for a metropolitan area like Atlanta. Furthermore,

these schemes require a line-of-sight (LOS) link from the base station antenna to the handset in order to work well. In rural areas, these technologies have difficulty reaching enough base stations to perform triangulation; in urban areas, the absence of LOS degrades the performance of this technology.

GPS-based solutions are quite accurate when LOS exists to at least three GPS satellites. But, this “open sky” condition exists only for some outdoor locations and never for indoor handsets. Another key problem with GPS-based schemes is that the GPS link is designed to work with SINR only a few dB above the noise floor. Any loss incurred by an obstruction (tree, terrain, building, indoor environment, in-vehicle environment, etc.) will knock out the radio link in conventional GPS. In addition, the GPS-based solution requires additional hardware and an out-of-band RF chain in a handset. Replacing all existing non-GPS handsets will take many years.

The LOS condition is crucial condition for time-based, angle-based, and GPS location solutions. Because most calls are made indoors, where no LOS exists, the indoor location problem cannot be avoided for E911 systems.

RSS-based solutions use RSS measurements of the forward control channel, transmitted by all base stations to find handsets. In TDMA (IS-136) systems, the mobile station can measure the power of up to 24 neighboring control channels. Unlike voice channels, the forward control channel is transmitted at a constant-power and yields a reliable, repeatable measurement. GSM systems report the 6 strongest control channels. In an RSS location scheme, No additional base station is required because RSS measurements are all information needed from the handset hardware. Furthermore, RSS location schemes do not require the existence of a LOS signal, which make them excellent solutions for suburban and urban areas and for indoor environments. The aim of this work is to prove the feasibility of RSS the scheme in these environments.

1.3 How RSSI-based Radiolocation Works

The operation of RSSI-based position location is straightforward. A cellular network area is represented in a computer by a large, two-dimensional raster array with uniform grid spacings of 10 to 50m. Each raster point in the grid corresponds to a location within the network and contains a vector of received signal strength indicator (RSSI) values in dBm for all audible base stations. Each RSSI is cross-referenced to a unique cell identification number, as shown in Figure 1.1. A complete raster array of RSSI is called a predicted signal database (PSD). Once a PSD has been constructed for a network area, the RSSI-based location engine must compare received signal strength measurements made by the handset to the PSD vectors. The best match determines the xy-coordinates of the most likely handset location.

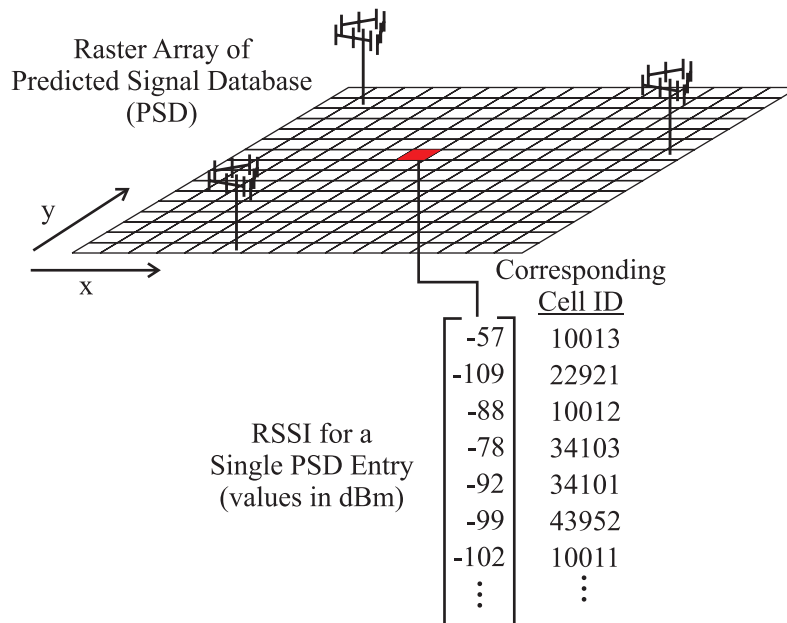


Figure 1.1 The Predicted Signal Data (PSD) stores a raster database of all RSSI from audible base stations within the network.

Handset RSSI measurements are taken from the user handset's network measurement report (NMR). NMRs are sent from the handset to the base station whenever requested by the mobile switching center (MSC). Each NMR is a list of many RSSI corresponding to the different radio channels on the network. The exact number of channels depends on handset location, network architecture, and air interface, but the typical size of an NMR ranges from 6 to 12 unique cells (GSM handsets usually report the strongest 6 cells while IS-136 handsets report typically between 8-12 cells or more, the exact number depending on a pre-programmed neighbor list provided by the serving cell). Since a handset's location consists of two pieces of information (x and y coordinates), the mapping of 6 or more RSSI values into this two-dimensional location space results in a significantly over-determined problem; the excess information helps to increase the accuracy and robustness of the RSS location estimate. In normal operation, a single NMR is generated whenever the handset initiates a call or performs a hand-off to another cell. By changing just a few settings at the base station's switch, it is possible to request a stream of NMRs during 911 emergency calls. Only one NMR is required to produce a handset location estimate, but a stream of NMRs is quite useful for averaging out residual fading effects at the receiver or tracking a handset in motion. Since the storage of a PSD and the operation of an RSS location engine require only a modest computer terminal, the entire position location system is a remarkably inexpensive and accurate method for E911 and location-based services.

A high-quality PSD is the crucial point for a successful RSS location solution. The more accurate the PSD, the better the location performance. The best PSD would be generated by measuring signal strength at every possible location in the network. But exhaustive measurement is impractical due to incredible manpower and time costs. This is particularly true if the RSS solution is extended to the indoor environment

unless good propagation models is applied.

1.4 Key Outcomes

This report presents experimental results for a RSS position location, which was performed on the Georgia Tech campus. Several key outcomes of this work are:

1. This is the first academic experiment to validate the performance of RSS location for the North American E911 system in general.
2. This study shows that, with regard to FCC-mandated performance statistics, indoor environments show little degradation of location performance when compared to a system where all handsets are outdoors.
3. Discrimination of outdoor and indoor handsets is possible. With proper algorithms and distribution statistics of indoor/outdoor measurements, the discrimination rate can reach up to 92%. (see Section 6.2.4)
4. We present several suggestions for algorithms that improve the location performance.

MEASUREMENT PLAN

All measurements were taken on the Georgia Tech campus, surrounded by the box in Figure 2.1. We selected a 700 m by 500 m region as our experimental test area. In this area 23 buildings were measured, marked by X's in Figure 2.1. There are three base stations inside the test area, where eight medium-tier sectors are in use. Another five base stations in the neighborhood also provided coverage for the edge of the test area. The distance between base stations was approximately 400-500 meters. The construction style for most of the buildings was steel and concrete with brick surfaces. Some of the buildings had glass walls. Terrain in this area was hilly with ground elevation differences of about 10 m from the peak to trough. Detailed building descriptions are given in Section 3.1. The roads in this area were mostly two-lane, two-way streets. The average population on workday is around 15,000 people. This is a typical semi-urban area, where radio location is problematic for angle-, time-, or GPS-based location technologies.

The measurement campaign lasted for 4 months, during this time the leaves grew back on the deciduous trees. The seasonal shift changed the wireless propagation environment, which degraded our calibrated predicted signal database (PSD). Thus, the experimental results are thought to be more pessimistic than using a timely

calibrated PSD.



Figure 2.1 Indoor/Outdoor “location laboratory” at Georgia Tech campus in semi-urban Atlanta, GA.

2.1 Setup Overview

Our measurement was performed with two different measurement tools. The data collected by different equipment generated two different databases. PSD calibration data was collected by a Comarco LT200 IS-136 RF scanner with baseband decoding. Handset data was collected by an Ericsson TEMS Light 3.0 unit. To measure as much as possible, drive-test measurements, outdoor walking measurements and indoor walking measurements were taken. Drive-test measurements provided a fast way to measure across a large outdoor area while walking measurements filled in the holes where the drive-test measurements could not access.

Each major campus building within the test area was measured using the following procedure.

1. The measurement system was calibrated before each measurement. This procedure is described in Section 2.2.
2. Outdoor drive-test measurements were made along the road using the Comarco LT200 unit. Drive-test measurement were kept at the speed of 15-20 km/hr (9-13 miles/hr). The received signal strength of each of the 26 digital control channels was measured.
3. Outdoor walking measurements are made around the building using the Comarco LT200 unit. Walking measurements are taken at the speed of 2-4 km/hr (1-2 miles/hr). RSS of each of the 26 digital control channels was measured. For details, see Section 3.2.
4. Indoor walking measurements were made in all the rooms on the edge of the buildings. If the room was less than 10 meters in length, the measurement was performed over a meandering path within the room during a 30-second period. If the length was longer than 10 meters, the measurement was performed along a straight line from one end of the room to the other with a constant speed of 2 km/hr.
5. At the end of the day, another hardware calibration was performed to verify the system integrity. This involves repeating measurements at two locations taken earlier in the day to verify system stability.
6. The measurement device was changed from the Comarco unit to the TEMS light 3.0 unit to collect handset testing data. This data is taken through an

ericsson handset that is strapped to the field engineers head for the most lifelike usage. Steps 1-4 were repeated to build up a database of test measurements.

2.2 Equipment and Calibration

2.2.1 Comarco LT200 Unit

The Comarco LT200 is a TDMA 800 and 1900 band scanner. Channel sets collected in our measurement campaign lied in the IS-136 800 MHz band, which were all digital control channels for the network that was measured. The handset used with the scanner is a NOKIA 2160. Figure 2.2 illustrated the scanner connection. Figure 2.3 is picture to show how the real scanner system connected.

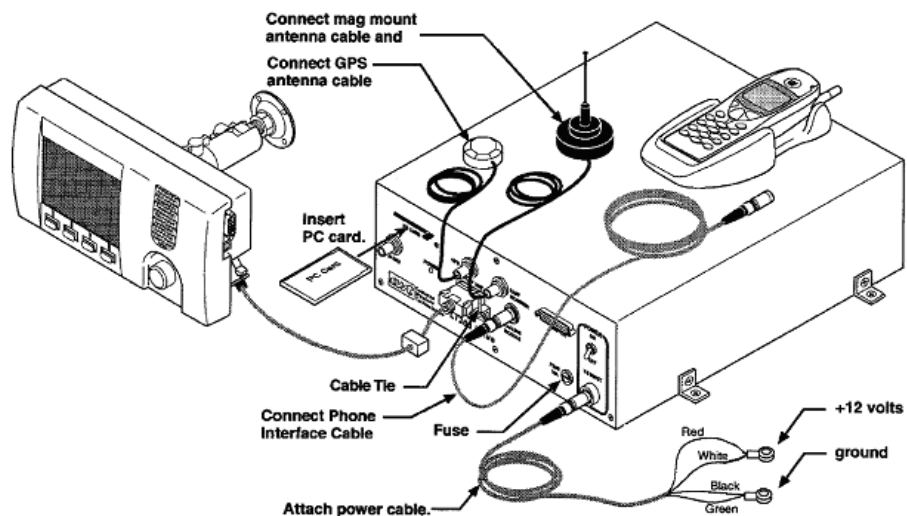


Figure 2.2 Scanner setup illustration (Comarco LT200 Users Guide[pg162]).

The specifications for the Comarco LT200 are as follows:

- On-line call RSSI with adjacent channels, along with three selected channels

with adjacents, once per second.

- RSSI for four best A and B system serving channels; digital control channel updated every 4 seconds.
- Wide dynamic range of
 - 20 to -110 dBm accuracy ± 1 dB
 - 110 to -120 dBm accuracy ± 3 dB
- Can scan all A and B band control channels once per second.
 - Channel-to-channel scan rate < 5 ms, typically 3 ms
- 21 channels of a selected or on-line channel set with SAT every 2 seconds

2.2.2 Ericsson TEMS Light 3.0 Unit

The Ericsson TEMS is a portable device for RF scanner and active call measurement. The hardware components of the TEMS light system include one ERICSSON TEMS handset and a FUJITSU STYLISTIC 1000 tablet PC . The total weight of this system is about 4.5 lb. This unit can scan up to 24 channels simultaneously. The scanning function was used to construct our handset test data. We programmed the 24 channels to correspond with the base stations closest to Georgia Tech.

2.2.3 Calibration Procedure

A standard free-space calibration procedure was employed on each day of RF measurement to monitor the integrity and consistency of our equipment. The calibration consisted of spatially-averaged power measurements taken on the roof top of the Van Leer building at the start and end of each day of RF field measurements. By bracketing each day of field measurement with this calibration procedure, we not only verified



Figure 2.3 Actual SComarco canner Setup.

the consistency of the RF equipment throughout the day, but can be alerted to any day-to-day biases within either the cellular network or our measurement setup.



Figure 2.4 Actual TEMS unit Setup.

The basic calibration procedure for the RSSI measurement system was as follows:

1. Define Calibration Paths: The location of the calibration location was on the 5th-floor rooftop of the Van Leer building on the campus of the Georgia Institute of Technology. Figure 2.5 shows the layout of the Van Leer building rooftop. The dashed line marked the calibration routes used in our experiment. Route 1 was a $40.6 \text{ m} \times 5.5 \text{ m}$ box-shaped path whose southwest corner had GPS coordinates of -84.39747° longitude and 33.77591° latitude. Route 2 was a straight 39.8 m line running east-west whose western endpoint had GPS coordinates of -84.39738° longitude and 33.77581° latitude. Although Georgia Tech was an urban campus, the rooftop of Van Leer places the equipment above most of the trees and smaller buildings that potentially block or distort GPS

measurements. Each calibration route was large enough to provide a variety of RSSI measurements within a local area, but small enough not to introduce significant large-scale variations in the average RF power.

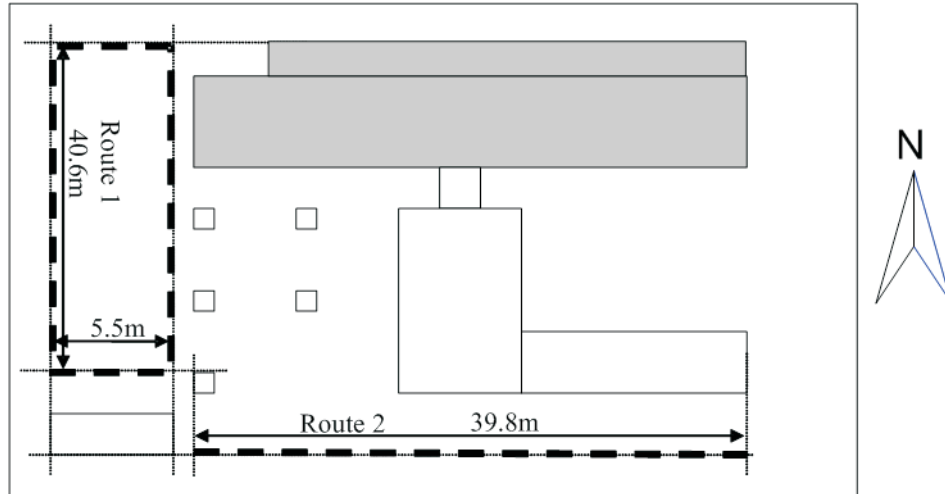


Figure 2.5 Rooftop Calibration Route.

2. System Setup: To begin a day of measurements, the RF measurement system was connected on top of the cart according to the block diagram of Figure 2.2. If a scanner measurement was being calibrated, the scanner's cellular antenna was placed on top of the cart in a vertical position. If an handset measurement is being calibrated, the handset was placed on the mounting pole anchored firmly to a stable board with a vertical orientation. The GPS antenna rested on top of the cart, separated from the cellular antenna and the handset by at least 20 cm. The scanner's display unit was also mounted on the stable board that was placed onto the scanner main body for easy movement. Since the scanner antenna and the GPS antenna have a magnetized base, a metal board was used for mounting.

3. **Acquire Data:** The equipment was set to measure using either the scanner or the handset. Data was acquired by moving slowly along Route 1. This was repeated along Route 2 so that two unique data sets are taken. Each route was measured in no less than 60 seconds to ensure sufficient amounts of data were logged.
4. **Post-processing:** The data was then immediately downloaded to a computer for analysis. The analysis was identical for both scanner and handset data. For every measured control channel measurement, the RSSI values taken around each calibration route were linearly-averaged to produce a single average signal strength measurement in dBm. four checks were performed at this point of the procedure:
 - [a] **Long-Term Consistency Check:** the average RSSI values were compared with those taken on previous days. If RSSI values differed from previous measurements by ± 3 dB, a thorough system check was performed.
 - [b] **Short-Term Consistency Check:** For an end-of-day calibration, average RSSI values were compared to the start-of-day calibration.
 - [c] **GPS Position Check:** GPS is operating is verified by comparing the readings to previous GPS measurements.
 - [d] **Record and Save Average RSSI Values:** The average values were dated and recorded for future use. In constructing an RSSI database that uses measurements spanning multiple days, it may be necessary to normalize each day's measurement against the calibrated measurements.
5. **Repeat Procedure:** The calibration procedure was repeated using the identical procedure at the end of a measurement day.

Here is an example of calibration calculation, in which a linear power average is used:

$$RSSI_{AVG} = 10 * \log_{10} \left(\frac{\sum_{i=1}^N 10^{RSSI_i/10}}{N} \right) \quad (2.2.1)$$

In the following example, several measurements were acquired for digital control channels (DCCH) 797 from the College of Computing base station (cell number 3078). Table 2.1 gives an example of 18 instantaneous scanner measurements of power from base station 3078. Small scale fading and other effects added a great deal of variability to the measurement. The peak power in Table was -58.4 dBm and the lowest power was measured to be -71.9 dBm. This was a difference of 13.5 dB. However, the linearly-averaged power from Equation 2.2.1 is -63.2 dBm, which is nearly constant from day to day at this location.

Table 2.1 Measurement data of DCCH 797 from CoC base station.

No.	1	2	3	4	5	6	7	8	9
RSS	-62.8	-59.5	-58.4	-59.1	-66.8	-65.3	-59.8	-66.3	-64.8
No.	10	11	12	13	14	15	16	17	18
RSS	-69.0	-70.3	-64.6	-71.9	-64	-64.6	-64.3	-66.3	-65.5

DATA COLLECTION

3.1 Building Construction

Building construction, especially the material and design of the exterior wall, determines the penetration loss of radio waves. To discriminate between indoor and outdoor calls, this penetration loss information is very useful. In this report, we give an analysis of penetration loss for each building. We also present the penetration loss for typical office buildings from a statistical point of view. The buildings in our experiment are mainly steel, concrete, and brick, which are the typical building materials for urban areas.

The sample of measured buildings, summarized by Table 3.1, represents typical construction practice in our experimental area. The buildings in Table 3.1 represent typical semi-urban commercial buildings. For several representative buildings, we present some details of construction and site information that provide a better understanding of the test area. These parameters include the following:

1. Construction material.
2. Building type.
3. Size and layout of the building.

Table 3.1 Building construction summary for Georgia Tech.

Number	Campus buildings in the test area	Construction Material	Stories
075	ARCHITECTURE (WEST)	STEEL/CONCRETE	3
076	ARCHITECTURE (EAST)	STEEL/CONCRETE/BRICK	3
085	VAN LEER (ECE)	STEEL/CONCRETE	5
086	BUNGER-HENRY	STEEL/CONCRETE	4
111	MASON (CE)	STEEL/CONCRETE/BRICK	5
145	SUSTAINABLE EDUCATION	STEEL/CONCRETE	3
081	HOWEY PHYSICS	STEEL/CONCRETE/BRICK	4
095	PETTIT MIRC	STEEL/CONCRETE/BRICK	2
050	COMPUTING (COC)	STEEL/CONCRETE/BRICK	4
066	CHERRY L EMERSON	STEEL/CONCRETE/BRICK	3
114	HOUSTON	STEEL/CONCRETE	2
104	WENN STUDENT CENTER	STEEL/CONCRETE/BRICK	3
123	STUDENT SERVICES	STEEL/CONCRETE	2
103	BOGGS CHEMISTRY	STEEL/CONCRETE	4
124	FERST CENTER THEATER	STEEL/CONCRETE/BRICK	2
135	MRDC	STEEL/CONCRETE	4
055	INSTRUCTIONAL CENTER	STEEL/CONCRETE/BRICK	3
056	WENN STUDENT CENTER	STEEL/CONCRETE/BRICK	3
057	STUDENT SERVICES	STEEL/CONCRETE	2
054	STUDENT CTR DECK	STEEL/CONCRETE	3

4. Type and proximity of the surrounding buildings and trees near the building.
5. Terrain surrounding each building.

3.1.1 Architecture (West)

Architecture (west) building, constructed in 1980, is a three-story building with no basement. On the south side is a big parking lot. The area is lightly wooded with decorative trees. The building has several mid-sized trees around the perimeter. The north side is lightly wooded; some bushes sit immediately next to the building. Half of the first floor is a big hall. A library and design lab are separated from the hall by a glass wall. The south and north wall is made of aluminum frame and expansive glass. The east and west wall are made of concrete. On the west side is a big entrance made of aluminum-framed glass.

Table 3.2 Building Construction of Architecture (West).

Building Name	ARCHITECTURE (WEST)
Data of Construction	1980
Exterior Facade	red brick
Window size	glass wall for N/S large window for E/W
External Dimensions	54 m by 37 m
Number of Floors	3
Basement Present	No
Surrounding Environment	lightly wooded
Nearby Buildings	east and west
Base Terrain	lightly hilly



Figure 3.1 South side of Architecture (West).

3.1.2 Architecture (East)

Architecture (East) building is a three-story building with a basement. It was built in 1952. On the south side is the Rich building, which has a base station on its roof. The building has several mid-sized trees to its south and east side. The Architecture (East) building is separated into two parts—a north unit and a south unit. The surface of the south unit is mainly brick, while the north unit is made from brick and large expanses of glass. The south and north sides of the north unit have glass walls.

3.1.3 Van Leer (ECE)

Van Leer is a five-story building with half of the first floor below the ground level. It was built in 1961. The surrounding area is lightly wooded. On the north side is another building MiRC (Microelectronics Research Center), which is only meters away from Van Leer. The signal from the base station atop the CoC building is

Table 3.3 Building Construction of Architecture (East).

Building Name	ARCHITECTURE (WEST)
Data of Construction	1952
Exterior Facade	red brick
Window size	glass wall for north unit small/no window for south unit
External Dimensions	56 m by 56 m
Number of Floors	3
Basement Present	Yes
Surrounding Environment	lightly wooded
Nearby Buildings	east and west
Base Terrain	extremely hilly

**Figure 3.2** North side of Architecture (East).

attenuated significantly by MiRC's blockage. The west and east sides of Van Leer have two major roads of Georgia Tech, Atlantic Drive and Plum St, which cut a path

for wireless signals to travel. Southside has a parking lot and a large lawn, which are both lightly wooded. Measurements were taken on the second floor because it is level with the ground on the west side of the building. Furthermore, the indoor area on the second floor is more accessible than that on the first floor, so the south side of this building was measured closely against the wall. At the other sides the preferred area for indoor data collection (indoors but as close as possible to the outside wall) was not accessible; only several offices were open. East and north sides were measured in the interior hallway instead, which may have introduced inaccuracy for calculating the angle-related penetration loss. The west side was measured in both the hallway and several offices.

Table 3.4 Building Construction of Van Leer (ECE).

Building Name	Van Leer (ECE)
Data of Construction	1961
Exterior Facade	red brick and glass wall with decorative concrete
Window size	small window offices, semi-glass wall at south side
External Dimensions	56 m by 88 m
Number of Floors	5
Basement Present	No
Surrounding Environment	lightly wooded
Nearby Buildings	north
Base Terrain	extremely hilly

3.1.4 Pettit MiRC

Pettit MiRC was built in 1988. It is a two-story building with a basement. The building is lightly wooded on all sides and sits on relatively hilly terrain. The first



Figure 3.3 South side of Van Leer (ECE).

floor has a lot of offices, each office has a size of 3 m by 4 m. Measurements were taken in most of the offices that are next to the outside wall at the west, south, and north side. Some offices on the north and south sides are inaccessible at the time of measurement. On the east side is a hallway where indoor measurements are taken against the outside wall. On the east side and west side of the building are two streets, Atlantic Drive and Plum Street. Wireless signals arriving from the south side will be blocked and scattered by Van Leer, which is immediately south of MiRC. On the north side is the CoC building, where a base station is mounted on the rooftop.

3.1.5 College of Computing (CoC)

CoC is a four-story building with the western part of the first floor below ground level. It was built in 1989. The building is lightly wooded and sits on extremely hilly terrain. It also sits between Atlantic Drive and Plum Street. A base station is

Table 3.5 Building Construction of Pettit (MiRC).

Building Name	Pettit MiRC
Data of Construction	1988
Exterior Facade	red brick
Window size	large window with shade
External Dimensions	58 m by 67 m
Number of Floors	2
Basement Present	Yes
Surrounding Environment	lightly wooded
Nearby Buildings	north and south
Base Terrain	relatively hilly



Figure 3.4 West side of Pettit (MiRC).

mounted on the rooftop of this building.

Table 3.6 Building Construction of College of Computing (CoC).

Building Name	College of Computing (CoC)
Data of Construction	1989
Exterior Facade	red brick
Window size	mid-size window
External Dimensions	60 m by 60 m
Number of Floors	4
Basement Present	No
Surrounding Environment	lightly wooded
Nearby Buildings	north and wouth
Base Terrain	extremely hilly

**Figure 3.5** West side of College of Computing (CoC).

3.1.6 Cherry Emerson

Cherry Emerson was built in 1959. It is a three-story building with no basement. The building is lightly wooded and sits on flat ground. Cherry Emerson is under direct



Figure 3.6 Northwest side of College of Computing (CoC).

illumination of the CoC base station from south. The other three sides are open areas; no buildings lie within 40 meters of Cherry Emerson. Measurements were taken on first floor. Most of the preferred areas close to the exterior walls were measured. This is a good site to study penetration loss for office buildings.

3.1.7 Howey Physics

The Howey Physics building was built in 1967. It is a four-story building that sits on hilly terrain. To the south is the civil engineering building (Mason). On the east side is the CoC building where a base station is mounted. The west side has a large parking lot, which is heavily wooded. The north side has a small parking lot. It is an open area. Measurements were taken on the second floor on the south side and on the first floor on the north side due to the hilly terrain.

Table 3.7 Building Construction of Cherry Emerson.

Building Name	Cherry Emerson
Data of Construction	1959
Exterior Facade	red brick
Window size	small window
External Dimensions	69 m by 26 m
Number of Floors	3
Basement Present	No
Surrounding Environment	lightly wooded
Nearby Buildings	south
Base Terrain	flat ground

**Figure 3.7** West side of Cherry Emerson.

3.1.8 Mason (Civil Engineering)

The Mason building is a combination of a 2-story building and a 5-story building. It was built on 1969. The base was built on relatively flat ground. On the north

Table 3.8 Building Construction of Howey Physics.

Building Name	Howey Physics
Data of Construction	1967
Exterior Facade	red brick
Window size	No window at south side, large window at north side
External Dimensions	94 m by 56 m
Number of Floors	4
Basement Present	No
Surrounding Environment	lightly wooded
Nearby Buildings	south
Base Terrain	hilly

**Figure 3.8** North side of Howey Physics.

side of the Mason building is the Howey Physics which is a large obstacle for wireless signals. The east side is facing the base station on top of CoC, while the south side

is also blocked by the Bunger-Henry building. On the west side is a large parking lot. Measurements were taken on the first floor. Most of the preferred areas were measured. This is a very good building to analyze penetration loss.

Table 3.9 Building Construction of Mason (Civil Engineering).

Building Name	Mason (Civil Engineering)
Data of Construction	1969
Exterior Facade	concrete and red brick
Window size	small/no windows, entrance is using glass wall
External Dimensions	78 m by 59 m
Number of Floors	5
Basement Present	No
Surrounding Environment	lightly wooded
Nearby Buildings	south and north
Base Terrain	flat



Figure 3.9 North side of Mason (Civil Engineering)).

3.1.9 Bunger-Henry

The Bunger-Henry building was built in 1964. It is a four-story building that sits on a slope. The north side has a small hill and the Mason building. The radio waves from the CoC building are scattered by the hilly terrain. The east side faces Atlantic Drive and the Van Leer building. Radio waves arriving from Atlantic Drive reach the Bunger-Henry building at a grazing angle. On the south side is heavily wooded lawn. The west side has a parking lot with a few trees. The line-of-sight for the radio signal travelling from the student center parking deck is blocked by the Ferst Center for Arts.

Table 3.10 Building Construction of Bunger-Henry.

Building Name	Bunger-Henry
Data of Construction	1964
Exterior Facade	concrete and red brick
Window size	small/no windows, entrance has glass wall
External Dimensions	47 m by 65 m
Number of Floors	4
Basement Present	No
Surrounding Environment	lightly wooded
Nearby Buildings	north
Base Terrain	hilly

3.1.10 Student Center Parking Deck

The Student Center Parking Deck was built in 1989. It is a three-level parking facility. The area is lightly wooded. The facility is sitting on a slight slope. The surrounding areas are relatively open. Only one building is within 80 meters of the student center



Figure 3.10 East side of Bunger-Henry.

Table 3.11 Building Construction of Student Center Parking Deck

Building Name	Student Center Parking Deck
Data of Construction	1989
Exterior Facade	concrete
Window size	small/large windows with no glass
External Dimensions	111 m by 78 m
Number of Floors	2 floor/3 levels
Basement Present	No
Surrounding Environment	lightly wooded
Nearby Buildings	northeast
Base Terrain	lightly hilly

parking deck, which is a Student Services building. A base station is mounted on the top level of this building.



Figure 3.11 East side of Student Center Parking Deck (medium-tier base station on utility pole on the corner of the structure.)

3.2 Outdoor Measurements

Outdoor measurements were used to calibrated PSD; They were also used to calculate the orientation-dependent penetration loss. The outdoor measurement campaign included two parts. The first part consisted of drive-test measurements, similar to those conducted by wireless service providers to optimize their networks. An RF scanner was placed in a vehicle so that RSSI information can be collected while the field engineer drives through the test area.

The second part of the data collection is walking measurements. Because drive test measurements are limited to roadways, the RSSI in a field close to a building or a pedestrian path cannot be measured by driving test. The field engineer pushed a handtruck on which the scanner was mounted. The scanner collected data while travelling the designed route. These pedestrian measurements do more than fill in the unmeasured areas of a network for RSSI radiolocation; they also allow measurement close-in to the test buildings, which allows the calculation of orientation-dependent penetration loss. This is discussed in Section 4.1.

3.2.1 Drive Test Measurement

Wireless service providers maintain their own drive-test measurement RSSI database for the purpose of optimizing their network. Their measurements are performed by their field engineering team. Recalibrating this database with fresh drive test measurements must be performed from time to time to ensure the system is working properly. Though this procedure costs manpower, it is a vital function for every carrier.

In our experiment, the goal for drive-test measurements is to calibrate our database of new RF maps for RSS location. By using this PSD, which is calibrated by drive

test measurements only, the location performance of an RSS location algorithm can be simulated. This simulation will also provide a baseline comparison of performance for more complicated PSDs that include indoor modelling.

A Comarco LT200 RF scanner was used in the drive test measurements. The vehicle was a sedan with the scanner antenna and GPS antenna placed on the rooftop, separated by 0.4 m. The collection vehicle moved at the speed of 20-25 kph. The measurement is shown in Figure 3.12.

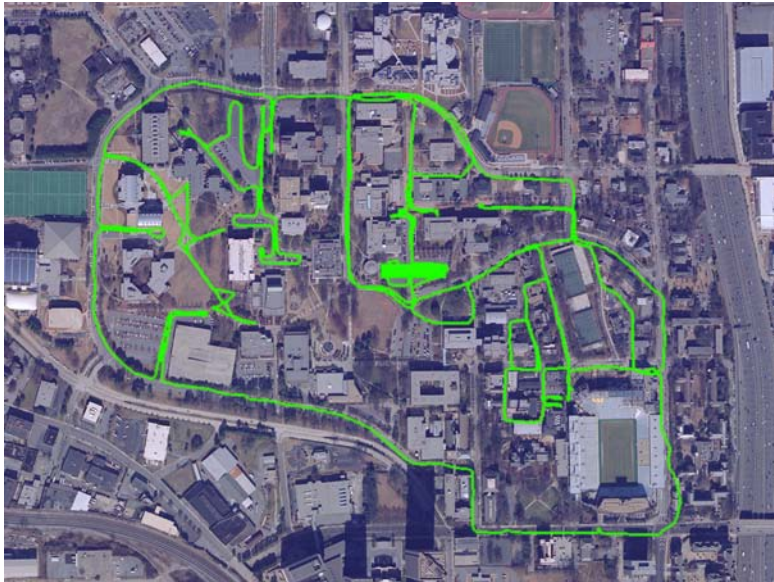


Figure 3.12 Driving route for outdoor drive-test measurement.

3.2.2 Walking Outdoor Measurement

A good outdoor walking measurement requires collecting the RSS data along the outside wall where a drive test measurement cannot reach. The goal of the walking measurement is to provide the RSS data for penetration model calculations and to provide a most accurately calibrated PSD. To calculate the penetration loss, the

signal strength at both sides of the building's outside wall is needed. The outdoor walking measurement result is used to generate an accurate PSD. Though this PSD is not practical in widespread commercial deployment of an RSS location system, it provides an upper limit of accuracy for these location methods.

After the PSD is calibrated, the handset data was collected using this same walking outdoor measurement. This collection procedure resembles a common cellphone user chatting with others while walking. Figure 3.13 and Figure 3.14 show typical outdoor walking measurements.



Figure 3.13 Georgia Tech student researcher Chris Durkin takes an outdoor walking measurement outside Bunger-Henry.

3.3 Indoor Measurements

All indoor measurements are taken at walking speeds. By studying both indoor walking measurements and outdoor walking measurements, the orientation-dependent



Figure 3.14 Georgia Tech student researcher Alenka Zajic takes an outdoor walking measurement outside student center parking deck.

penetration model can be calculated. (See Section 4.1.3) The indoor measurement is also used in calibrating the most accurate PSD. Figure 3.15 and Figure 3.16 show typical indoor walking measurements. Figure 3.17 shows that the handset is strapped to the field engineers head for the most lifelike useage.

The procedure for indoor measurement is as following:

1. Select the building. Find as much indoor area as possible against the outside wall that is accessible to measurement.
2. Select the measurement route for the building such that the route allows measurement on both sides of the exterior building wall.
3. Decide a measurement route in each room that is as straight as possible, parallel to the exterior wall.



Figure 3.15 Georgia Tech student researcher Joshua Griffin takes an indoor walking measurement inside Howey physics.

4. Mark the route on a map and record the start time of each route.
5. Move along the route at a constant speed. If the route is less than 10 meters, move backward and forward several times to make sure the measurement time lasts at least 30 seconds
6. Record the end time of the route.
7. Repeat 4-6 for all routes within the same building working around the perimeter as the floor plan permits.

Figure 3.18 shows the preferred indoor and outdoor measurement route. Figure 3.19 shows the actual measurement route in the Architecture building.



Figure 3.16 Georgia Tech student researcher Albert Lu takes an indoor walking measurement inside Architecture (East).



Figure 3.17 Georgia Tech student researcher Jian Zhu takes an handset walking measurement inside Van Leer.

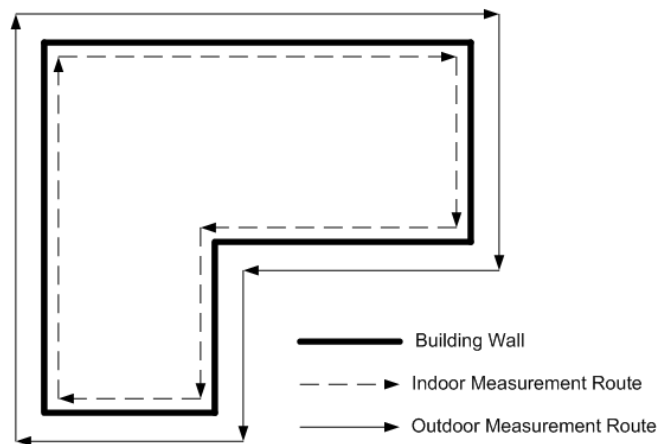


Figure 3.18 Indoor / outdoor measurement procedure measurement route.

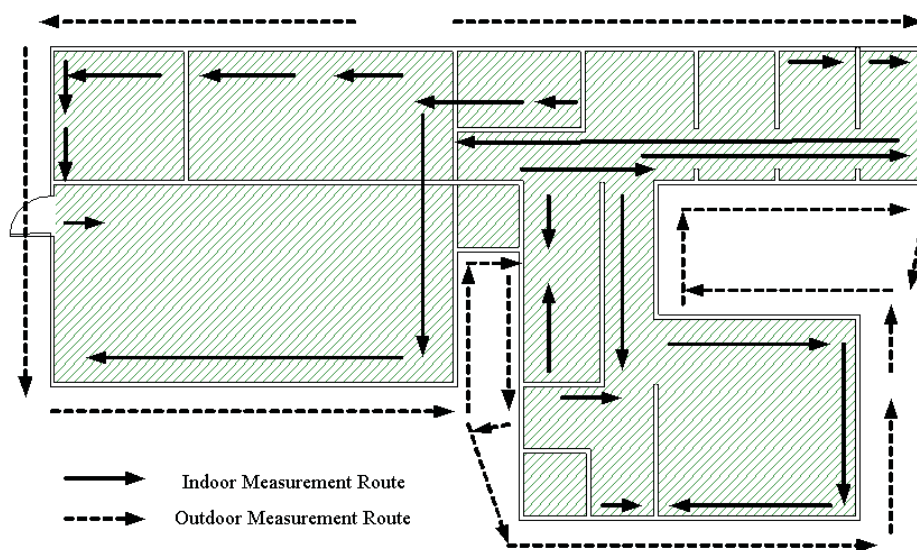


Figure 3.19 Measurement Route Record at Architecture Building.

3.4 GIS Data

The location experiments in this report use *geographical information systems* (GIS) data to assist in the indoor and outdoor location of users. The principle source of GIS in the study is a high-resolution database of aerial photographs of the city of Atlanta. This GIS image contains photographic pixels with $1\text{ m} \times 1\text{ m}$ resolution. The image was constructed in 2002 – nearly one-and-a-half years prior to the measurement campaign.

The aerial photographs were used to construct highly accurate building footprints of the test area on campus. First, the GIS photographs were digitally cropped. By manually associating two outdoor points on the map with their corresponding latitudes and longitudes, as measured by GPS, all pixels on the photograph can be georeferenced. Using typical imaging software, the buildings in the photographs were manually traced and filled to create a building footprint map. Although this act was performed manually, there are a number of computer algorithms and GIS companies that also provide this type of processing.

The end result of this image processing is a high-resolution binary map that distinguishes (in two-dimensions) coordinates that are indoors and outdoors. Figure 3.20 shows a sample output of this step. The map is based on recent city photographs; however, several modifications were made in cases of new or demolished buildings. The footprint map is then subsampled to $10\text{m} \times 10\text{m}$ resolution to match and align with the RF maps used in the experiments. This building footprint map is used for indoor propagation modeling and the location algorithm itself.

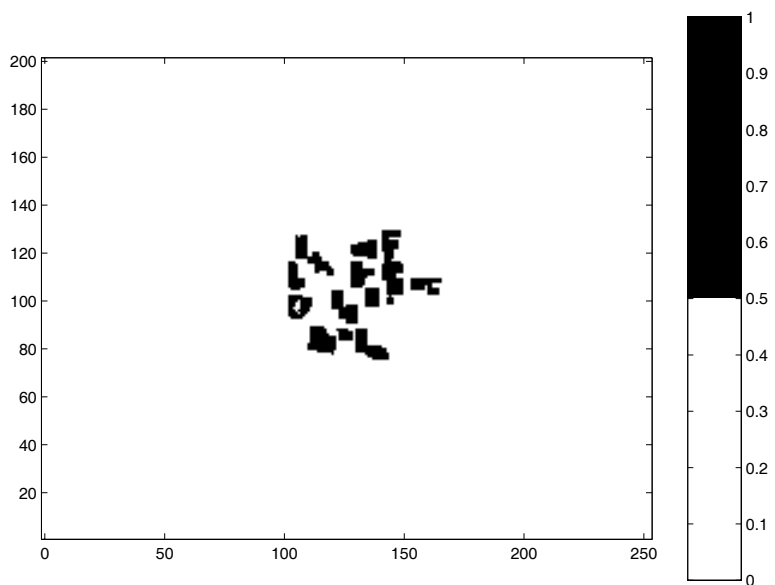


Figure 3.20 Binary building footprint inside experiment area.

DATA ANALYSIS

4.1 Angle-Related Penetration Loss

This section presents the methodology for modeling losses for cellular radio waves penetrating buildings.

4.1.1 Basics of Indoor Propagation

The signal strength measured by an indoor wireless handset depends on the propagation characteristics of the building. Regardless of the type of building – office, home, factory, store, etc. – the propagation characteristics of the *outdoor* environment also affect the indoor received signal strength. For that reason, it is usually best to model penetration relative to the path loss immediately surrounding the building [Dur98].

There are several attributes of indoor propagation that may assist RSS radiolocation if modeled correctly. These include:

- **Initial Loss:** A radio signal in cellular bands experiences an immediate loss upon penetrating a typical building. This value varies from building-to-building, but it is common to use single-value averages to estimate the loss [Agu94].
- **Orientation Dependence:** Of particular importance to location estimation algorithms is the ability to model the effects of building orientation with re-

spect to the serving base station. A transmitter that illuminates the side of a building directly experiences a different penetration loss than a transmitter that illuminates the side of a building at a grazing angle. Capturing this property in a model is what enables a location engine to discriminate position based on relative signal strengths from different base stations.

- **Layered Loss:** As a rule-of-thumb, total path loss increases for handsets further inside a building. Indoor walls and partitions screen the propagating waves as they penetrate into the building. This is a higher-order effect that may be too difficult to contribute to the performance of a location engine.

Since it is highly impractical to make measurements of all indoor environments, RSS location must rely on modeling these indoor penetration characteristics to some degree.

4.1.2 Indoor Propagation Issues for RSS Location

We should note that there are three different questions to ask in an indoor radiolocation study, each corresponding to different types of location technology. The first question is *can we discriminate between indoor and outdoor cellular users?* The second question is *can we correctly discern in which building an indoor cellular user is making a call?* The third question is *can we pinpoint the position of an indoor cellular user within a building?* From a technical point of view, these questions are presented in order of increasing difficulty. And each affirmative answer represents a unique location service.

Interestingly, these three questions correspond nicely to the basic indoor propagation characteristics described in Section 4.1.1. It would be valuable in E911 applications to discriminate between an indoor or outdoor cellular user – even if the

exact building could not be discerned. This could be done by comparing RSS measurements to the initial or average propagation loss of buildings. Section 6.2 presents this analysis for our experiment.

Discerning the exact building of an indoor user is more difficult, and pinpointing users within a building even moreso. Success in these two tasks would require an extremely detailed database of indoor and outdoor RF maps. In the absence of exhaustive measurement, *orientation dependence* and *layered loss* are crucial for this type of indoor radiolocation.

4.1.3 Octant Model of Orientation Loss

In our study, we desire to tabulate how penetration loss changes as a function of building incidence with respect to a cellular base station. From physics, we expect normal-incident waves to propagate into a building with less loss than grazing incidence. Thus, if we were to compare received powers in cellular handsets operating on opposite sides of a exterior building wall (one indoors and one outdoors), we would not expect the difference in measured power for each control channel to be the same. Since different control channels originate from different base stations and propagate through a building exterior with dissimilar angles of incidence, the penetration loss will differ for each. If this difference is pronounced, it may be possible to model and exploit this effect in RSS radiolocation.

Average values for building penetration loss for cellular bands are well-tabulated[Ber94]. How these losses change as a function of orientation is not well understood. There are a number of physical mechanisms and factors that affect the orientation-dependence of penetration loss. Polarization of the incident radio wave, electrical properties of the building exterior, material inhomogeneities, and surface roughness all affect orientation-dependent penetration loss. And although the most powerful radio waves

emanate from the direction of the base station, multipath propagation implies that the arriving angles of many radio waves are dissimilar to the base station bearing angle. From a physics standpoint, calculating orientation-dependent penetration loss is hopeless.

Empirical values for orientation-dependent penetration loss are not nearly so challenging. By studying propagation around and into a variety of typical buildings, representative values can be calculated. One useful way of organizing and tabulating this data is to use the octant model, illustrated in Figure 4.1. Essentially, incident angles are divided into 8 uniformly-spaced octants. Unique penetration loss values are calculated and assigned for each octant. Although it may seem crude, the octant model is a useful way to characterize and report orientation-dependent penetration loss. As an added benefit, there are some modeling algorithms that use octant data to model penetration loss [Dur03].

The octant corresponding to a range of incident angles is recorded as an integer value. This integer value ranges from 1 to 5 (not 1 to 8 because of symmetry), as shown in Figure 4.1. Qualitatively, each octant of incidence corresponds to the following propagation:

- 1 **Near-Normal Incidence:** The radio wave is arriving at near-normal incidence to the surface of a building. This type of propagation is, on average, the least-lossy mode of radio signal penetration into the building.
- 2 **Oblique Incidence:** The radio wave arrives at an oblique angle with respect to the building surface (neither perpendicular nor parallel). This type of propagation is lossier than near-normal incidence.
- 3 **Grazing Incidence:** The radio wave arrives at an incident angle that is nearly parallel to the surface of the building. This type of propagation should be very

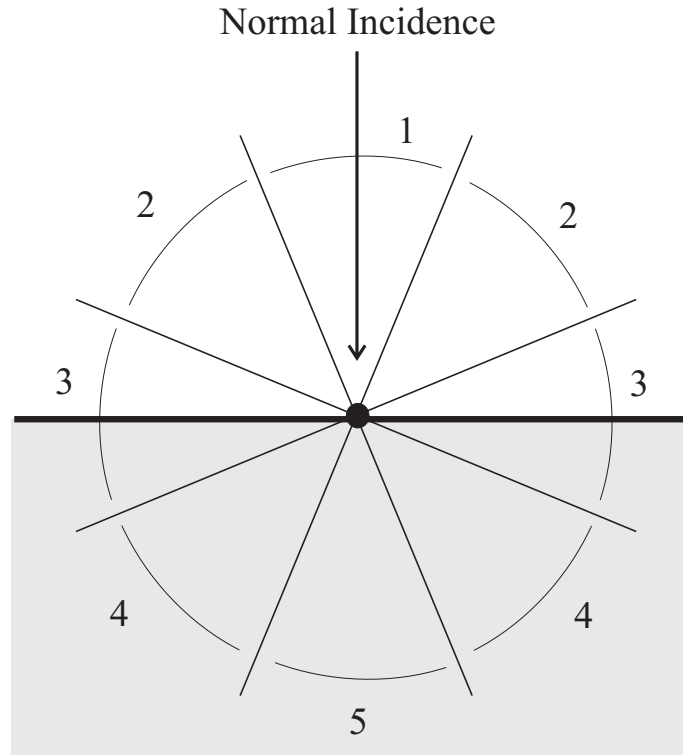


Figure 4.1 Directions are broken into uniform angle ranges called *octants*. The thick line is the building surface. Above is outdoors, below is indoors.

lossy, unless a significant amount of scatterers exist outside the immediate area of the building.

4 **Oblique Backscatter:** The base station illuminates the surface from an oblique angle on the *opposite* side of the building. The resulting penetration loss should be high.

5 **Near-Normal Backscatter:** The base station illuminates the surface from a direction *opposite* the building surface. The resulting penetration loss should be high, but not necessarily the highest; the surface is nearly normal to much

of the back-scattered power [Dur02].

The next section discusses octant model values obtained from our extensive building measurements.

4.1.4 Octant Penetration Values

Table 4.1 Octant penetration values.

Octant	1	2	3	4	5
Loss (dB)	7.5	8.3	8.9	9.3	9.2

In Table 4.1, the lowest penetration loss is 7.5 dB and the highest penetration loss is 9.3 dB, a difference of only 1.8 dB. The 850MHz propagation does not appear to depend on incidence angle as much as 1900MHz. This may make location of an indoor handset within a particular building nearly impossible.

4.1.5 Building Sample Analysis

In this section, we present an example of penetration loss calculated for one control channel power. The Architecture (east and west) building is under direct illumination from the Rich building base station, which is 20 meters away to the south. The sector facing the architecture building is using digital control channel 792.

The wall at area H8-N9 is solid red brick. There are no windows. The penetration loss is about 13-18 dB. The wall at area B6-G7 is a metal-framed glass wall, the penetration loss is lower, at 8-13 dB.

The Van Leer building reflects much of the power into the A1-B7 area. Received signal for the outdoor part of A1-A7 is mainly coming from scattering and reflecting from Van Leer while the indoor RSS at B1-B7 is mostly due to signals penetrating through wall B6-G7. The area of M6-N8 is similar to A1-B7.

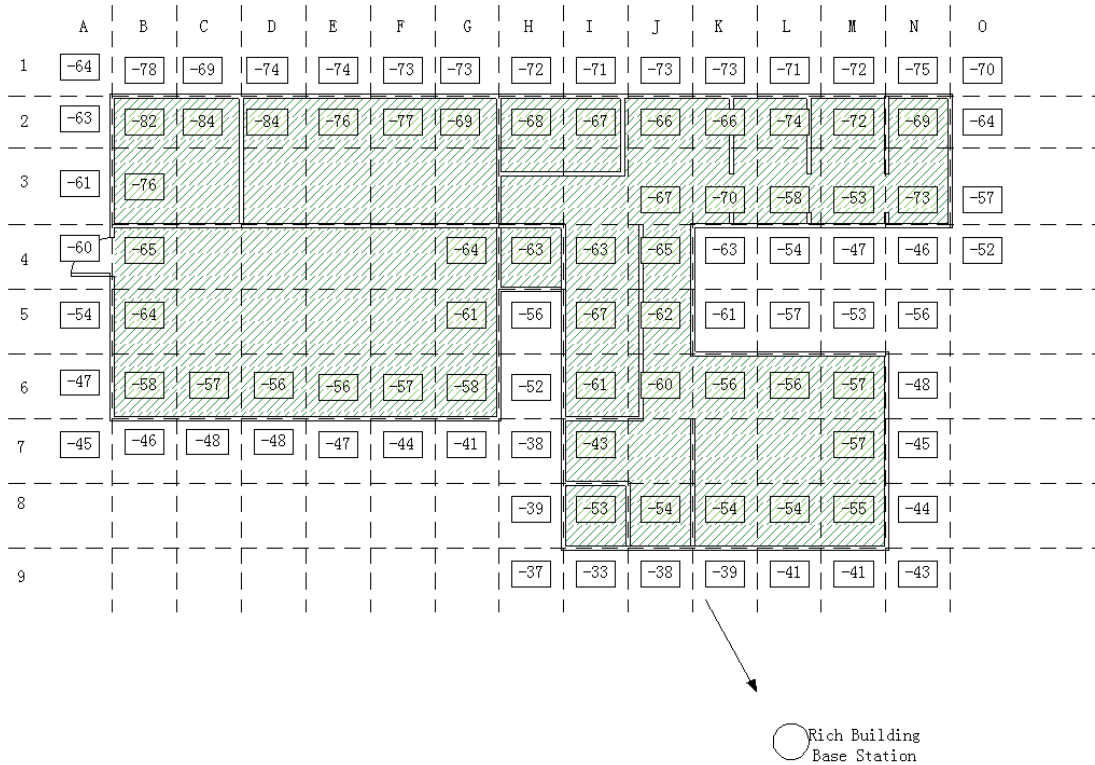


Figure 4.2 RSS at Architecture Building.

The wall in area A1-O2 is mainly glass and there is no direct illumination; the Delta Tau Delta building reflects radio waves into this part of building. The radio waves for the outdoor B1-N1 area are coming from secondary scattering and reflection from the edge of the Architecture, Van Leer, and Delta Tau Delta buildings. The indoor signal for area B2-N2 is a combination of the outdoor waves travelling through the glass wall and the waves propagating through the building.

4.2 Handset RSS Distribution

In our experiment, we found that the information used to discriminate between the indoor and outdoor calls is mainly embedded in the absolute value of the RSS. Ac-

curate distributions of RSS from indoor and outdoor callers can be used to calculate whether a call comes from indoors or outdoors.

4.2.1 Indoor RSS Distribution

This section shows the distribution of indoor power measurement taken from the handset data collection. Based on these handset measurements, we calculated the average RSS over the six strongest channels, which we call the *received signal strength aggregate* (RSSA). Because RSSA measured at a handset is affected by several different factors, such as distance, user head effects, penetration loss of different materials, and measurement noise, we can assume the distribution of summation of the six strongest channels is log-normal. Figure 4.3 and Figure 4.4 provides good evidence for this assumption. Figure 4.4 show that the log-normal assumption is a good model for the distribution of received signal strength for outdoor handsets. In the indoor case, the second peak results from the nonlinearity of the handset RF chain. The handset can only measure signals with strengths higher than -113 dBm. For all the strength levels lower than or close to -113 dBm, the nonlinearity of the handset RF chain will report several dB higher than the actual received signal. This makes all the data points lower than -110 dBm collapse to -110 dBm and form the small second peak. Despite this effect, the major trend of measurement statistics still matches up to the theoretical distribution.

Based on our experiment, the mean of indoor RSSA is -97.8 dB and the standard deviation is 14.1 dB. The statistics from the measurement and the theoretical distributions are shown in Figure 4.3.

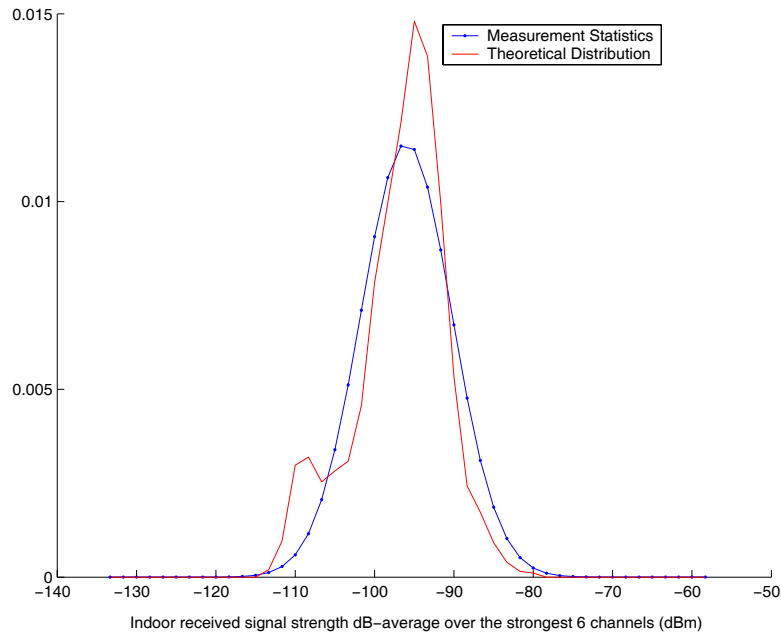


Figure 4.3 Indoor Received Signal Strength Aggregate (RSSA) distribution measured at Georgia Tech campus.

4.2.2 Outdoor RSS Distribution

Based on the handset data, the mean is -85.5 dB and the standard deviation is 9.7 dB. The statistics from the measurement and the theoretical distributions are shown in Figure 4.4

4.2.3 Indoor/Outdoor Comparison

Figure 4.5 shows the difference between indoor calls and outdoor calls in side-by-side plots. Interestingly, there is a large standard deviation of indoor RSSA (14.1 dB) when compared to outdoor RSSA (9.7 dB). The mean indoor RSSA is 12.3 dB lower than the outdoor RSSA. If gains and losses in the handset RF chain are similar, then it may be possible to discriminate between indoor and outdoor handset using RSSA.

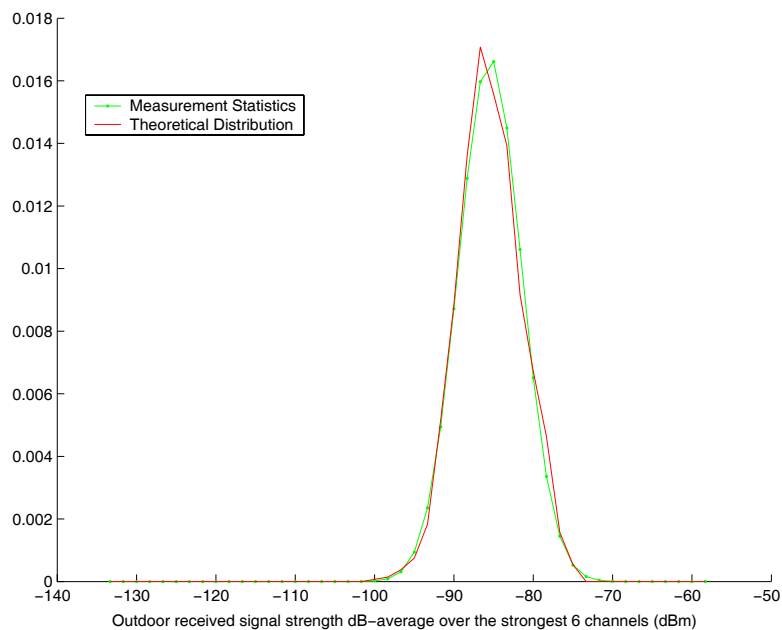


Figure 4.4 Outdoor Received Signal Strength Aggregate (RSSA) distribution measured at Georgia Tech campus.

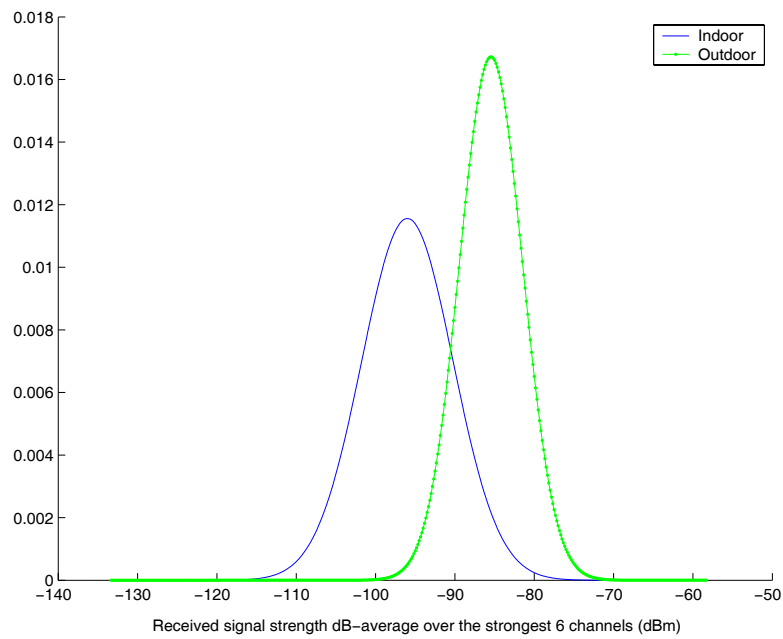


Figure 4.5 Indoor and outdoor RSSA theoretical distribution.

PREPARING RF MAPS

5.1 Introduction

For our location experiments, we generate PSDs from RF coverage maps with 3 different levels of measurement calibration: 1) outdoor measurements only, 2) outdoor and indoor measurements, and 3) outdoor measurements and indoor propagation modeling. The same position location algorithms are run using these 3 different PSDs. This three-fold testing procedure demonstrates the level of calibration required to meet accuracy targets in the location engine.

Each PSD is constructed from these different sets of RF coverage maps. Regardless of which 3 PSDs are used in the analysis, the construction of the RF maps follows a similar procedure in every case. This procedure is discussed in the following sections.

5.2 Simple Propagation Modeling

The first step in preparing RF maps is to, make a base map from a simple propagation model. A base RF map is constructed from network information provided by the carrier. This information includes base station longitude and latitude, sector antenna orientation, frequency channel, and transmit power.

The basic propagation prediction technique used to make the initial RF maps

follows the same procedure in every case. All pure signal strength predictions are based on a modified version of the Hata model [Rap02]. The radio link budget used for this type of link is given below:

$$P_R = P_T + G_R + G_T \cos(\theta - \theta_b) - 10n \log_{10} \left(\frac{d}{1 \text{ m}} \right) - 20 \log_{10} \left(\frac{4\pi}{\lambda} \right) + C_{\text{dB}} \quad (5.2.1)$$

where the terms in Equation (5.2.1) are summarized as follows:

- P_R - power received by a handset (dBm)
- P_T - power transmitted by a sector (dBm)
- G_R - estimated handset antenna gain (0 dBi)
- G_T - estimated peak sector antenna gain (7 dBi)
- θ - bearing angle of predicted location (degrees)
- θ_b - sector antenna bearing angle (degrees)
- d - separation distance (m)
- n - path loss exponent (3.3)
- λ - wavelength of radiation (m)
- C_{dB} - constant offset (dB)

The variable C_{dB} in Equation (5.2.1) is a constant offset term that accounts for additional gains and losses due to antenna height and pattern, RF hardware, frequency offset, or any other consistent, unmodeled effects in the RF chain. The value for C_{dB} is chosen to minimize the standard deviation error between the raw modeling and any drive test measurements corresponding to the sector. In this manner, we construct every raster RF map at $10\text{m} \times 10\text{m}$ resolution for each sector in and around the campus of Georgia Tech. A modeled estimate of signal strength, P_R , is placed at every raster point in an RF map.

An example of a base RF map made from the pure modeling of Equation (5.2.1) is shown in Figure 5.1. The map is crude and lacks much of the texture and detail

of more realistic RF maps. Enhanced propagation modeling may be used to improve the accuracy of the RF maps. For this experiment, however, extensive outdoor measurements in the test area make accurate modeling less important. The RF maps become more accurate after they are *interpolated* with measurements.

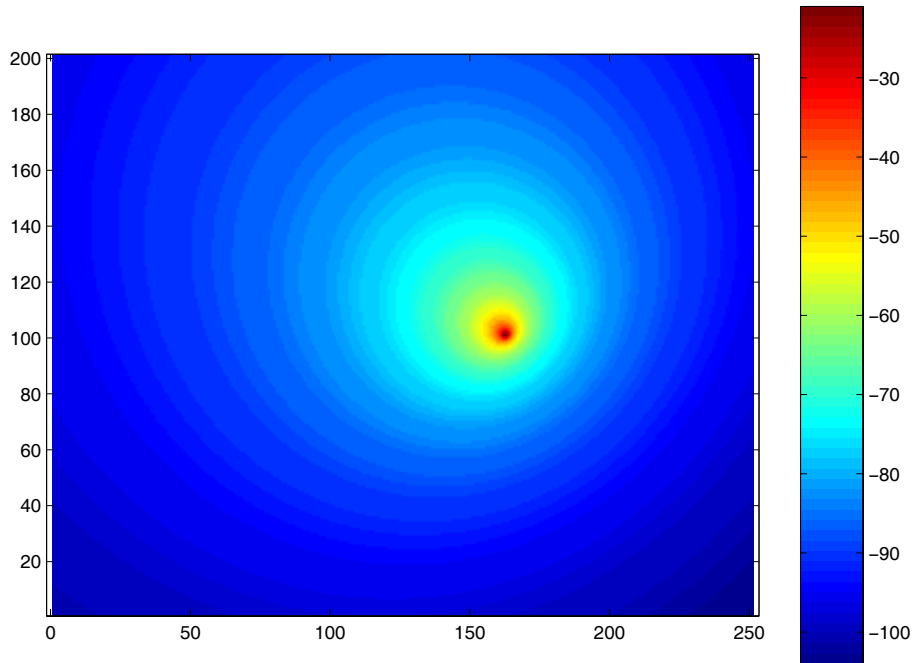


Figure 5.1 RF map based on pure prediction using a modified Hata model.

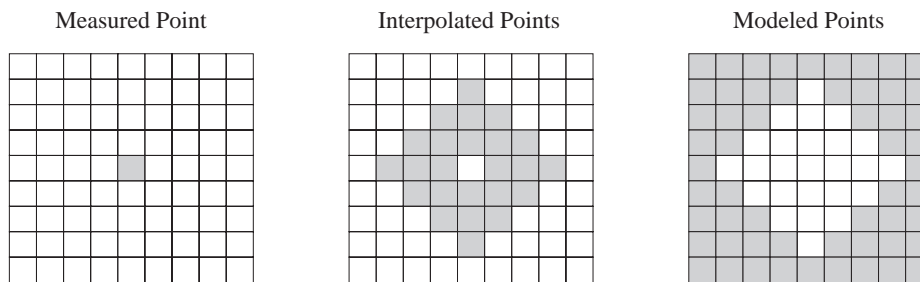
5.3 Interpolating Measurements into RF Maps

The next step in the production of a PSD is to blend measured data into the RF maps. At locations in the map where measured data exists, it is preferable to substitute the measured signal strength in place of the modeled signal strength. In map areas that are far from measured points, we are forced to rely on purely modeled signal strength. For areas in an RF map that are several raster points away from measured

data points, we use a weighted combination of the modeled values and the value of nearby measurement point. This process of blending modeled signal strength with nearby measurements is called *local interpolation*.

There are many imaginable schemes for local interpolation. The scheme used in our RF maps is a 2D cubic interpolation scheme over a diamond-shaped area that surrounds every measured raster point. The difference between measured, interpolated, and modeled signal strength regions is illustrated in Figure 5.2. Enlarging the radius of the diamond around each measurement point leads to more aggressive interpolation. All RF maps in this study use interpolation with a radius of 3 raster points (30 meters) from measurement center.

(a) Single Measurement Point



(b) Measurements Taken Along a Path

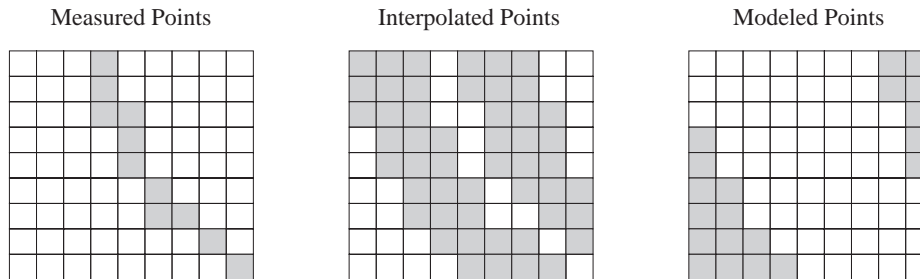


Figure 5.2 Marked raster regions (in gray) for (a) a single measurement and (b) a path of measurements.

It should be noted that most measured points do not occur in isolated regions as illustrated in the upper part of Figure 5.2. Measured data points tend to cluster along paths due to the walking or driving methods of collection. For this reason, the lower part of Figure 5.2 represents a more realistic separation of interpolation regions. For clusters or paths of measured points, the diamond-shaped interpolation region are cumulatively masked together for every single collected point.

Also note that each measured point is actually the linear average of every instantaneous RF scanner measurement made at a frequency whose longitude and latitude happen to fall within the $10\text{m} \times 10\text{m}$ raster point. This effectively removes any small-scale fading effects or other anomalies in the collection procedure. Drive-test measured points typically have 3 to 5 instantaneous power measurements averaged within a single raster point. Pedestrian collections typically have 5 to 15 (or more) averaged power measurements due to the slower collection speed.

5.4 Three Types of Databases

In this section we describe in greater detail the three types of PSDs used in the location experiments.

5.4.1 Outdoor Measurements (Level 1)

The first PSD is calibrated with only outdoor measurements, specifically those collected through drive-testing. All indoor and pedestrian outdoor collections are omitted from this PSD. Furthermore, there is no attempt to model signal penetration through buildings. This type of RF map database represents the general purpose RSS position location solution proposed in [PB00],[Rao99]. It is the most practical solution since all measured signal strength data can be collected using standard

cellular drive test procedures. Thus, the data collection is quick and economical.

An example of an RF map used in a Level 1 PSD is shown in Figure 5.3. Note the additional detail in the received signal strength when compared to the pure modeling map of Figure 5.1. This additional measurement detail is smoothly blended into the modeled regions using interpolation.

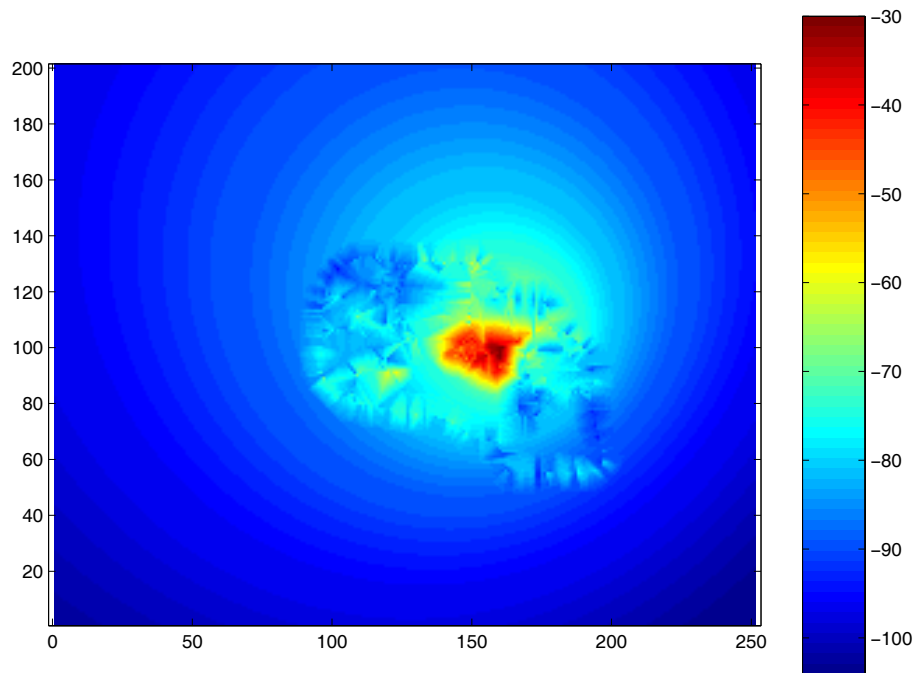


Figure 5.3 RF map calibrated with outdoor drive test measurements for use in a Level 1 PSD. (Map units in dBm.)

5.4.2 Outdoor Measurements and Indoor Modeling (Level 2)

The second PSD is calibrated with outdoor measurements and indoor modeling. While the outdoor portions of the RF map are similar to the Level 1 PSD, raster points corresponding to indoor locations are modified with additional loss based on

the model described in Section 4.1. This model is calculated from a simple, geo-referenced map of building footprints on the campus of Georgia Tech. Since these footprint maps are readily available in nearly all urban and suburban areas, the Level 2 PSD is also practical and economical to construct.

An example of an RF map used in a Level 2 PSD is shown in Figure 5.4. The dark blocks in this RF map are areas of low signal strength typical of indoor cellular use.

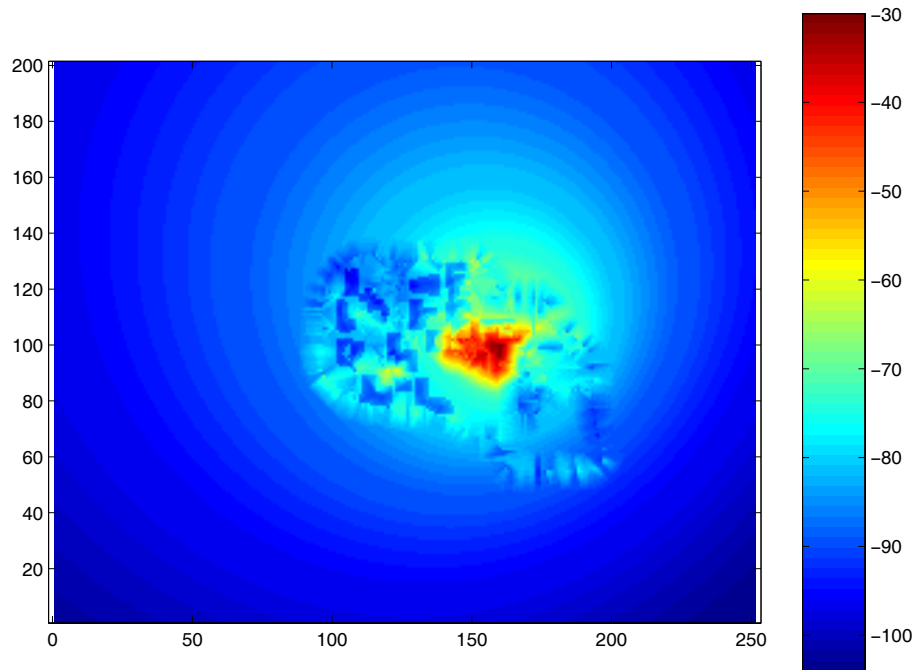


Figure 5.4 RF map calibrated with outdoor drive test measurements and indoor modeling for use in a Level 2 PSD. (Map units in dBm.)

5.4.3 Outdoor and Indoor Measurements (Level 3)

The Level 3 PSD is constructed from extensive outdoor and indoor measurements. Due to the difficulties, time, and expense of taking indoor measurement, this particular PSD is not very practical for widespread deployment. Calibrating a database of RF maps with indoor measurements may only be economical in several critical areas. For E911 applications, this may be inside several downtown buildings that have a high density of cellular users (hotels, conference halls, office buildings, etc.) Location experiments run with a level 3 PSD are particularly useful, however, as they illuminate the upper-limit of performance for an indoor/outdoor location algorithm.

An example of an RF map used in a Level 3 PSD is shown in Figure 5.5. The signal strength map of Figure 5.5 looks very similar to the signal strength map of Figure 5.4. This is highly desirable as we want our indoor propagation model to mimic the behavior of the indoor measurements.

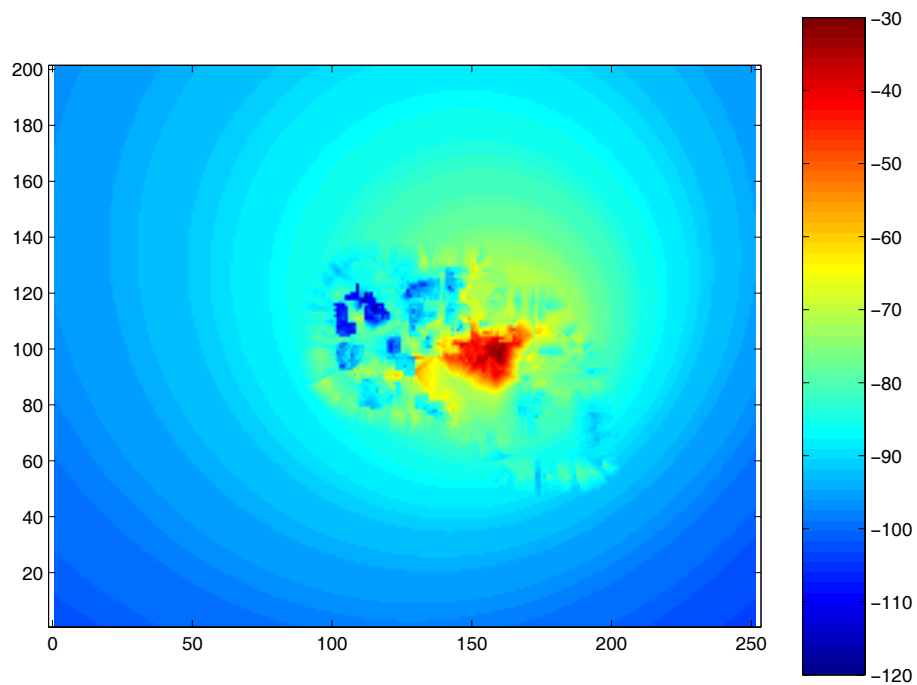


Figure 5.5 RF map calibrated with outdoor and indoor measurements for use in a Level 3 PSD. (Map units in dBm.)

LOCATION PERFORMANCE

6.1 Overview of Location Algorithm

This section describes the basic concept of Euclidean distance used to estimate handset location.

6.1.1 Definition of M-Distance—Euclidean Distance

In order to solve for the location of a handset, we must design an algorithm for matching received signal strength measured by a handset (reported in an NMR) with received signal strength recorded in a PSD. In this experiment, we base our location algorithm on the *Euclidean distance* between a set of measured and recorded signal strengths. We call this the *matching distance*.

Each NMR is like a point in multi-dimensional space. A handset NMR that contains N received signal strength measurements is like a point in N -dimensional space. This is also true for the collection of signal strengths in a PSD. Each physical xy location modeled in the Georgia Tech campus PSDs contain up to 26 received signal strength values, each corresponding to different IS-136 800 MHz control channels. From these values, a location algorithm selects a subset of N values that corresponds to the same control channels present in the NMR. Thus, we need a general formula

for calculating the matching distance between two N -length vectors of received signal strength.

If an NMR reports signal strengths from N control channels, then we may represent this measurement as a vector of length N :

$$[Nr_{ss_1} \ Nr_{ss_2} \ \cdots \ Nr_{ss_N}] \quad (6.1.1)$$

where Nr_{ss_i} is the reported signal strength of the i th control channel. Likewise, we may construct a similar vector for each discrete xy location in a PSD:

$$[Pr_{ss_{x,y,1}} \ Pr_{ss_{x,y,2}} \ \cdots \ Pr_{ss_{x,y,N}}] \quad (6.1.2)$$

where $Pr_{ss_{x,y,i}}$ is the predicted signal strength of the i th control channel at the xy coordinate. The matching distance M is calculated with the following formula:

$$M_{x,y} = \sqrt{\sum_{i=1}^N (Pr_{ss_{x,y,i}} - Nr_{ss_i})^2} \quad (6.1.3)$$

The coordinates xy that yield the lowest matching distance are chosen to be the location estimate.

6.1.2 Metric of Location Performance

To judge the location performance we use the following two standards to measure the accuracy of our system.

- Location Error Statistics
- Indoor/Outdoor Discrimination Rate

Location Error Statistics

The distance in meters between a location estimate and the handset's groundtruth position is the *error distance*. To understand the true performance of any location

algorithm, we must study this error distance for many location attempts. The FCC requirements for E911 accuracy place several conditions on the cumulative distribution of error distance. Specifically, the error distance must be less than 100m for 67% of the time and less than 300m for 95% of the time. Thus, for every location experiment in this study, we calculate and report the percentages of error distance values below 100m and 300m.

Indoor/Outdoor Discrimination Rate

For each location estimate, we attempt to discern whether the handset is either indoors or outdoors. We refer to this process as *indoor/outdoor discrimination*. The discrimination *rate* is the percentage of handsets that have been correctly identified as either indoors or outdoors. Indoor/outdoor discrimination is an important piece of information for emergency services.

6.1.3 Dart-Throwing Probability

The reader must keep in mind that discrimination rates may look deceptively successful at first glance. If told that a location algorithm could discriminate between indoor and outdoor users 60% of the time, then one might suppose that this algorithm was somewhat successful. However, one could achieve 50% success simply by flipping a coin. With this in mind, the 60% success rate does not seem nearly as impressive.

To place all reported indoor/outdoor discrimination rates in proper perspective, they must be accompanied by a *dart-throwing probability*. The dart-throwing probability is the success rate for discerning indoor handsets from outdoor handsets by randomly choosing locations on the building footprint map (i.e. “throwing a dart at the map”). Presumably, this is the worst possible method for discriminating the location of handsets.

According to our definition of the discrimination rate, success occurs under two different conditional outcomes of a location experiment: 1) when an indoor handset is detected to be indoors or 2) an outdoor handset is detected to be outdoors. Furthermore, each of these outcomes must be weighted against the probability of being indoors or outdoors. In mathematical terms, we can write this as:

$$\text{Success} = Pr[P = I|M = I]Pr[M = I] + Pr[P = O|M = O]Pr[M = O] \quad (6.1.4)$$

$$\text{Error} = Pr[P = O|M = I]Pr[M = I] + Pr[P = I|M = O]Pr[M = O] \quad (6.1.5)$$

where M denotes the true (measured) position of the handset and P denotes the predicted position of the handset. The variables M and P both have only two types of outcomes: O for outdoors or I for indoors. By the conditional probability theorem, we may rewrite these equations as

$$\text{Success} = Pr[P = I \& M = I] + Pr[P = O \& M = O] \quad (6.1.6)$$

$$\text{Error} = Pr[P = O \& M = I] + Pr[P = I \& M = O] \quad (6.1.7)$$

In a dart-throwing decision (one made without information), prediction and measurement are independent events and, hence, multiplicative. Thus, the dart throwing success and failure rate is given by

$$\text{Success} = Pr[P = I]Pr[M = I] + Pr[P = O]Pr[M = O] \quad (6.1.8)$$

$$\text{Error} = Pr[P = O]Pr[M = I] + Pr[P = I]Pr[M = O] \quad (6.1.9)$$

The calculation for probabilities $Pr[P = I]$ and $Pr[P = O]$ are based on the fraction of indoor and outdoor geometrical area that exists on a building footprint map, respectively. The calculation for probabilities $Pr[M = I]$ and $Pr[M = O]$ is based on the fraction of indoor and outdoor groundtruth locations used in the testing.

6.2 Performance

In this section we discuss the performance of several different location algorithms. Unless otherwise noted, each NMR is constructed from the 8 strongest measured sectors collected from the Ericsson handset.

6.2.1 Absolute RSS Location

The first location algorithm to test is based on absolute signal strength. In the absolute RSS location algorithm, we assume perfect knowledge of the antenna/RF chain bias between the user handset and the scanner used to calibrate the PSD. This bias is removed by subtracting a bias constant from every signal strength reported in the NMR.

$$Nrssc_i = Nrssi - \text{Bias} \quad (6.2.1)$$

where $Nrssc_i$ is the unbiased received signal strength of the i th reported control channel. This unbiased set of measurements is then matched to the PSD. The unbiased NMR is used to calculate the matching distance for each raster point as in Equation (6.2.2).

$$M = \sqrt{\sum_{i=1}^N (Prss_{x,y,i} - Nrssc_i)^2} \quad (6.2.2)$$

The location performance is summarized in Table 6.1 and Table 6.2. Without indoor modeling, the experiment shows an abysmal discrimination rate of 32% – statistically equal to the dart-throwing probability. However, when the indoor model is introduced to the PSD, the success rate of indoor/outdoor discrimination jumps to 78%. For a PSD with extensive indoor measurements, this rate improves to 86%. The absolute RSS location algorithm can discern indoor and outdoor handsets admirably with either indoor modeling or measurement.

The error statistics in Table 6.2 are also promising. In fact, the Level 3 PSD meets FCC requirements for E911. The Level 1 PSD is sufficiently worse.

Table 6.1 Discrimination rate of the absolute RSS location algorithm. (Dart-throwing probability of 34%.)

PSD level		Level 1 Outdoor Meas.		Level 2 Indoor Model		Level 3 Indoor/Outdoor Meas.	
		Decision					
		Indoor	Outdoor	Indoor	Outdoor	Indoor	Outdoor
Actual	Indoor	270	2993	2818	454	2837	416
	Outdoor	394	1343	657	1071	270	1477
Correct Rate		32%		78%		86%	

Table 6.2 Location error statistics of absolute RSS location algorithm.

PSD level		Level 1 Outdoor Meas.		Level 2 Indoor Model		Level 3 Indoor/Outdoor Meas.	
Error statistics	<100m	20%	45%	67%			
	<300m	60%	90%	95%			

6.2.2 Relative RSSI Location

For the relative RSS location algorithm, the measurements in an NMR and the signal strengths in the PSD are normalized before matching. The normalization procedure is described below:

- First, we extract all received signal strength values from the PSD that correspond to the control channels reported in an NMR. This gives us vectors in the form of Equation (6.1.2) and Equation (6.1.1).

- The mean of each vector in the PSD is calculated in dBm. This mean is subtracted from the vector:

$$Prssr_{x,y,i} = Prss_{x,y,i} - \frac{1}{N} \sum_{j=1}^N Prss_{x,y,j} \quad (6.2.3)$$

where $Prssr_{x,y,i}$ is the received signal strength of the i th control channel at the location coordinates x and y .

- The mean of the measured NMR vector is subtracted from the measured vector to form a new vector:

$$Nrssr_i = Nrss_i - \frac{1}{N} \sum_{j=1}^N Nrss_j \quad (6.2.4)$$

where $Nrssr_i$ is the received signal strength reported in the NMR in the i th channel.

After normalization, all vectors of received signal strength become independent of any Antenna/RF chain bias.

The relative signal vectors from the NMR and PSD are used to calculate the measurement distance for each raster point as in Equation (6.2.5).

$$M(x, y) = \sqrt{\sum_{i=1}^N (Prssr_{x,y,i} - Nrssr_i)^2} \quad (6.2.5)$$

The smallest measurement distance point (x',y') is the location estimation. Relative RSS algorithms do not require the perfect knowledge of the bias of the handset antenna/RF chain, which makes this algorithm more realistic.

The location performance is summarized in the Table 6.3 and Table 6.4. As Table 6.3 demonstrates, the relative RSS algorithm cannot discriminate between indoor and outdoor users, regardless of the level of PSD construction. This is not too surprising. Since the bias constant of a handset's RF chain is indistinguishable from the

average loss due to building penetration, subtracting the mean value gets rid of the most useful piece of information for discerning the position of indoor handsets.

The overall error statistics in Table 6.4 look promising, however. There seems to be little difference in performance between the 3 levels of PSD. All three come close to achieving the FCC requirements for E911 in this semi-urban environment.

Table 6.3 Discrimination rate of relative RSS location algorithm. (Dart-throwing probability is 34%)

PSD level		Level 1		Level 2		Level 3	
		Outdoor Meas.		Indoor Model		Indoor/Outdoor Meas.	
		Decision					
		Indoor	Outdoor	Indoor	Outdoor	Indoor	Outdoor
Actual	Indoor	849	2401	739	2511	1334	1916
	Outdoor	436	1314	417	1333	528	1222
Correct Rate		43%		41%		51%	

Table 6.4 Location Error Statistics of Relative RSS location algorithm

PSD level		Level 1		Level 2		Level 3	
		Outdoor Meas.		Indoor Model		Indoor/Outdoor Meas.	
Error statistics	<100m	54%	54%	54%	54%	60%	60%
	<300m	94%	94%	94%	94%	95%	95%

6.2.3 Hybrid-Method RSS Location

The hybrid-Method takes advantage of the robust relative RSS method for locating the handset, but studies the absolute signal value as well to discern indoor/outdoor information. The discrimination algorithm is based on the *received signal strength*

aggregate (RSSA) method discussed in Section 4.2. After some statistics, we have the knowledge for RSS distribution for indoor scenario and outdoor scenario, as showed in Figure 4.5.

By using this information, we can calculate the probability for an active call coming from indoor or outdoor. Refer to Figure 6.1 for the following discussion.

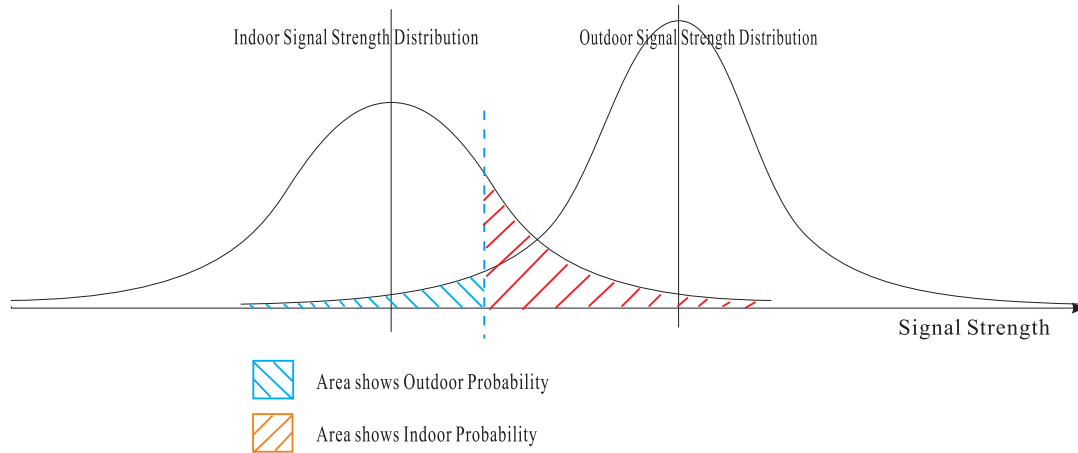


Figure 6.1 Calculation the probability of indoor call or outdoor call from RSSA

Let μ_i denote the mean of the sum of the strongest 6 channels for an indoor handset. Let σ_i denote the standard deviation of this same sum. Let μ_o denote the mean of the sum of the strongest 6 channels for outdoor handsets. Finally, let σ_o denote the variance of the strongest 6 channels for outdoor handsets. The distribution of indoor RSSA for the strongest 6 channels is

$$p(x) = \frac{1}{\sigma_i \sqrt{2\pi}} e^{-(x-\mu_i)^2/(2\sigma_i^2)} \quad (6.2.6)$$

The distribution of the outdoor RSS for the strongest 6 channels is

$$p(x) = \frac{1}{\sigma_o \sqrt{2\pi}} e^{-(x-\mu_o)^2/(2\sigma_o^2)} \quad (6.2.7)$$

The probability that the indoor RSSA is greater than a value x is given by

$$P_i(x) = \frac{1}{\sigma_i\sqrt{2\pi}} \int_x^{-\infty} e^{-(x-\mu_i)^2/(2\sigma_i^2)} dx' = \frac{1}{2} \left[1 - \operatorname{erf}\left(\frac{x-\mu_i}{\sigma_i\sqrt{2}}\right) \right] \quad (6.2.8)$$

The probability that the outdoor RSSA is less than a value x is given by

$$P_o(x) = \frac{1}{\sigma_o\sqrt{2\pi}} \int_{-\infty}^x e^{-(x-\mu_o)^2/(2\sigma_o^2)} dx' = \frac{1}{2} \left[1 + \operatorname{erf}\left(\frac{x-\mu_o}{\sigma_o\sqrt{2}}\right) \right] \quad (6.2.9)$$

where $\operatorname{erf}()$ is the so-called error function

$$\operatorname{erf}(z) = \frac{2}{\sqrt{\pi}} \int_0^z e^{-(t)^2} dt' \quad (6.2.10)$$

From these equations, we can estimate the probability that a given RSSA is more likely to be indoors or more likely to be outdoors.

The normalization procedure and the location method are exactly the same as in the relative RSS location algorithm. After the location estimate is made, the RSSA is calculated to decide whether the handset is indoors or outdoors. If the raster point (x,y) is indoors:

$$M_H(x, y) = M(x, y) / P_i\left(\sum_{i=1}^N Nr_{ssr_i}\right) \quad (6.2.11)$$

If (x,y) is an outdoor point:

$$M_H(x, y) = M(x, y) / P_o\left(\sum_{i=1}^N Nr_{ssr_i}\right) \quad (6.2.12)$$

The point xy with the smallest hybrid measured distance, M_H , is the location estimate.

The location performance is summarized in Table 6.5 and Table 6.6. Because the hybrid method is using RSSA instead of PSD information to decide whether a handset is indoors or outdoors, the discrimination rate is the same – 90% – for all 3 types of PSD. This is quite promising.

The error statistics for this location algorithm are also promising. The Level 1 PSD results in position estimates that are 100m from groundtruth 56% of the time and 300m from groundtruth 96% of the time. The Level 3 PSD is even closer to the FCC specification. The Hybrid-Method algorithm seems to have improved both discrimination and error statistics.

Table 6.5 Discrimination rate of Hybrid-Method RSS location algorithm. (Dart-throwing probability is 34%.)

PSD level		Level 1 Outdoor Meas.		Level 2 Indoor Model		Level 3 Indoor/Outdoor Meas.	
		Decision					
		Indoor	Outdoor	Indoor	Outdoor	Indoor	Outdoor
Actual	Indoor	2895	334	2892	337	2909	320
	Outdoor	167	1604	167	1604	175	1596
Correct Rate		90%		90%		90%	

Table 6.6 Location error statistics of Hybrid-Method RSS location algorithm

PSD level		Level 1 Outdoor Meas.		Level 2 Indoor Model		Level 3 Indoor/Outdoor Meas.	
Error statistics	<100m	56%	56%	56%	56%	65%	65%
	<300m	96%	96%	96%	96%	96%	96%

6.2.4 Hybrid-Method RSS Location with Averaging

Until now, all location estimates have been performed with single NMRs. However, with several switch modifications at a base station, it is often possible to capture a sequence of consecutive NMRs for position location. The received signal strength in

these consecutive NMRs may then be linearly averaged to get rid of any small-scale fading in the handset.

Table 6.7 and Table 6.8 show results of a hybrid-method algorithm operating on a linearly-averaged set of 10 NMRs. The results are outstanding, as the discrimination rate has climbed to 92% and the error statistics for Level 2 and 3 PSDs satisfy (within statistical error) the FCC safety mandate.

Table 6.7 Discrimination rate of Hybrid-Method RSS location algorithm. (Linear averaging of 10 NMRs, dart-throwing probability of 34%.)

PSD level		Level 1 Outdoor Meas.		Level 2 Indoor Model		Level 3 Indoor/Outdoor Meas.	
		Decision					
		Indoor	Outdoor	Indoor	Outdoor	Indoor	Outdoor
Actual	Indoor	637	53	642	48	641	49
	Outdoor	28	282	34	276	44	266
Correct Rate		92%		92%		91%	

Table 6.8 Location Error Statistics of Hybrid-Method RSS location algorithm. Linear averaging of 10 NMRs.

PSD level		Level 1 Outdoor Meas.		Level 2 Indoor Model		Level 3 Indoor/Outdoor Meas.	
Error statistics	<100m	61%	64%	78%			
	<300m	97%	98%	98%			

6.2.5 Hybrid-Method RSSI Location for only 6 Sectors

The previous algorithm results are based on a total of 8 sectors reported in an NMR. This is somewhat below the average number of control channel powers reported in IS-136. GSM, however, is a similar TDMA-style air interface and reports the 6 strongest sectors. Thus, we repeat the hybrid method analysis for 6 sectors instead of 8 to demonstrate the applicability of the technology for GSM.

Table 6.9 reports discrimination rates for the single NMR, 6-sector case. Each level of PSD has a success rate of 86-87%, which is comparable to the 90% achieved with 8 sectors. The error statistics in Table 6.10 also show similar performance for all 3 levels of PSD. This performance falls a little short of the US E911 requirements.

Table 6.11 reports discrimination rates for the case of 10 linearly averaged NMRs with 6-sectors reporting received signal strength. The values are nearly identical to the single-NMR case in Table 6.9, suggesting that discrimination performance is unaffected by averaging out small-scale fading. This is not surprising since computing an RSSA in the hybrid method likely averages out fading among the different control channels. The error statistics for the 10-NMR, 6-sector case reported in Table 6.12 are similar to 10-NMR, 8-sector case in the previous section. This suggests that the strongest 6 received signals contribute the bulk of accuracy to the overall system performance.

6.2.6 Pure Outdoor Location Performance

To understand how much RSS location degrades for an indoor environment, we also run the RSS location engine with pure outdoor handset data and compare results with the cases above, in which the experimental handset database consists of two-thirds indoor sample points. This pure outdoor location is run under the same conditions

Table 6.9 Discrimination rate of Hybrid-Method RSS location algorithm. (Single NMR, 6 sectors, dart-throwing probability of 34%.)

PSD level		Level 1 Outdoor Meas.		Level 2 Indoor Model		Level 3 Indoor/Outdoor Meas.	
		Decision					
		Indoor	Outdoor	Indoor	Outdoor	Indoor	Outdoor
Actual	Indoor	2761	490	2762	489	2813	438
	Outdoor	197	1552	190	1559	220	1520
Correct Rate		86%		86%		87%	

Table 6.10 Location error statistics of Hybrid-Method RSS location algorithm. (Single NMR, 6 sectors)

PSD level		Level 1 Outdoor Meas.		Level 2 Indoor Model		Level 3 Indoor/Outdoor Meas.	
Error statistics	<100m	52%	53%	57%			
	<300m	93%	93%	93%			

as the experiments summarized by Table 6.9 and Table 6.10 (single NMR, 6 sectors of data, Hybrid location method.)

Table 6.13 shows solid indoor/outdoor discrimination performance between 82% and 85%. Table 6.14 shows that *every level of PSD is capable of meeting the FCC E911 requirements.*

Table 6.11 Discrimination rate of Hybrid-Method RSS location algorithm with averaging. (Linear averaging of 10 NMRs, 6 sectors, dart-throwing probability of 34%.)

PSD level		Level 1 Outdoor Meas.		Level 2 Indoor Model		Level 3 Indoor/Outdoor Meas.	
		Decision					
		Indoor	Outdoor	Indoor	Outdoor	Indoor	Outdoor
Actual	Indoor	610	72	618	64	620	62
	Outdoor	57	261	62	256	67	251
Correct Rate		87%		87%		87%	

Table 6.12 Location error statistics of Hybrid-Method RSS location algorithm with averaging. (Linear averaging of 10 NMRs, 6 sectors.)

PSD level		Level 1 Outdoor Meas.		Level 2 Indoor Model		Level 3 Indoor/Outdoor Meas.	
Error statistics	<100m	62%	63%	70%			
	<300m	96%	96%	96%			

Table 6.13 Discrimination rate of Hybrid-Method RSS location algorithm.

PSD level		Level 1 Outdoor Meas.		Level 2 Indoor Model		Level 3 Indoor/Outdoor Meas.	
		Decision					
		Indoor	Outdoor	Indoor	Outdoor	Indoor	Outdoor
Actual	Outdoor	741	4259	807	4193	885	4115
Correct Rate		85%		84%		82%	

Table 6.14 Location error statistics of Hybrid-Method RSS location algorithm.

PSD level		Level 1 Outdoor Meas.	Level 2 Indoor Model	Level 3 Indoor/Outdoor Meas.
Error	<100m	66%	67%	72%
statistics	<300m	97%	97%	97%

CONCLUSIONS

The results in this report demonstrate the feasibility of RSS location techniques to meet the FCC's requirements for E911 accuracy. The techniques remain accurate, even when the majority of test data is from *indoor* handsets. Since most mobile phone calls are now placed from inside buildings, inclusion of indoor data in any evaluation of an E911 location system is absolutely necessary. Although the vicissitudes of indoor radio wave propagation degrade the performance slightly, much of the accuracy can be recovered through a number of techniques presented in this report: averaging multiple NMRs, modeling indoor propagation, calibrating RF maps with indoor measurements, and trying different location algorithms.

Even more interesting is the unique ability of an RSS location engine to discriminate between indoor and outdoor handsets. This could prove to be a very important additional piece of information when dispatching help to the scene of an emergency. The highest success rate for indoor/outdoor discrimination in this experiment was 92/optimistic if there is a wild variability in the RF chains of commercial handsets. The variability of measurement bias in commercial handsets should be investigated further.

Although the results in this report were developed on a live IS-136 cellular network at 850 MHz, the performance is likely similar to other cellular telephony air interfaces

(GSM, CDMA, WCDMA, etc.) and other carrier frequencies. Future work for these techniques should concentrate on accurate propagation modeling and measurement, which enhance location performance regardless of air interface. Propagation modeling will be increasingly important as RSS location systems are deployed. Accurate propagation models reduce the time and cost of extensive drive-testing and also catch modifications to coverage when the cellular network undergoes optimization or build out. Good propagation practice undergirds this entire technology.

ACKNOWLEDGEMENT

The authors would like to thank Comarco Wireless Technology for their generous donation of a Comarco LT200 Scanner, which was the workhorse of this experiment. Comarco Inc. members Malcolm Levy, Louis Valbuena, and Willem Matins were especially helpful.

Thanks to Joshua Griffin, Chris Durkin, Alenka Zajic, and Albert Lu for many hours in the field helping with the measurement campaign.

Thanks to the Image Lab in the architecture department for their help in obtaining the latest version of campus aerial photographs.

The authors would also like to thank Polaris wireless Inc. for their technical suggestions and advice for this project.

BIBLIOGRAPHY

- [Agu94] S. Aguirre, L.H. Loew, and Lo Yeh, “Radio Propagation into Buildings at 912, 1920, and 5990 MHz Using Microcells,” in *Proceedings of 3rd IEEE ICUPC*, Oct 1994, pp. 129–134.
- [Aso00] M. Aso, T. Saikawa, and T. Hattori, “Mobile Station Location Estimation Using The Maximum Likelihood Method in Sector Cell Systems,” in *Vehicular Technology Conference 2002-Fall. Proceedings. IEEE 56th*, Sept 2000, vol. 2, pp. 1192 – 1196.
- [Aso01] M. Aso, M. Kawabata, and T. Hattori, “A New Location Estimation Method Based on Maximum Likelihood Function in Cellular Systems,” in *Vehicular Technology Conference 2001 Fall. IEEE VTS 54th*, 2001, vol. 1, pp. 106 – 110.
- [Ber94] H.L. Bertoni, W. Honcharenko, L.R. Maciel, and Howard H. Xia, “UHF Propagation Prediction for Wireless Personal Communications,” *Proceedings of the IEEE*, vol. **82**, no. 9, pp. 1333–1359, Sep 1994.
- [Caf98] J. Jr. Caffery and G.L. Stuber, “Subscriber location in cdma cellular networks,” *IEEE Transactions on Vehicular Technology*, vol. **47**, no. 2, pp. 406 – 416, 1998.
- [Caf00] J. Jr. Caffery, “A new approach to the geometry of toa location,” *Vehicular Technology Conference, 2000*, vol. **4**, pp. 1943 – 1949, 2000.
- [Che02] Yongguang Chen and Hisashi Kobayashi, “Signal Strength Based Indoor Geoloca-

- tion,” in *Communications, 2002. ICC 2002. IEEE International Conference on*, May 2002, vol. 1, pp. 436 – 439.
- [Chr00] R. Christ and R. Lavigne, “Radio Frequency-based Personnel Location Systems,” in *Security Technology, 2000. Proceedings. IEEE 34th Annual 2000 International Carnahan Conference on*, Oct 2000, pp. 141 – 150.
- [Dur98] G.D. Durgin, T.S. Rappaport, and H. Xu, “Partition-Based Path Loss Analysis for In-Home and Residential Areas at 5.85 GHz,” in *IEEE GLOBECOM 98*, Sydney, Australia, Nov 1998.
- [Dur02] G.D. Durgin, *Space-Time Wireless Channels*, Prentice Hall Inc., to appear in 2002.
- [Dur03] G.D. Durgin, “Location Estimation of Wireless Terminals Using Indoor Radio Frequency Models.,” *Patent filed on*, December 2003.
- [Klu98] R. Klukas and M. Fattouche, “Line-of-sight Angle of Arrival Estimation in The Outdoor Multipath Environment,” *Vehicular Technology, IEEE Transactions on*, vol. 47, no. 1, pp. 342 – 351, Feb 1998.
- [Kos00] H. Koshima and J. Hoshen, “Personal Locator Services Emerge,” *Spectrum, IEEE*, vol. 37, pp. 41 – 48, Feb 2000.
- [Lai01] H. Laitinen, J. Lahteenmaki, and T. Nordstrom, “Database Correlation Method For GSM Location,” *Vehicular Technology Conference 2001 Spring. IEEE VTS 53rd*, vol. 4, pp. 2504 – 2508, May 2001.
- [PB00] L. Perez-Breva, C.-Y. Chong, R. M. Dressler, P. R. Rao, P. Siccardo, and D. S. Spain, “Location and Determination Using RF Fingerprinting,” *U.S. Patent No. 6,393,294*, 22 Issued to *Polaris Wireless Inc.*, March 2000.
- [Rao99] P. R. Rao, “Multiple Location Estimates in a Cellular Communication System,” *U.S. Patent No. 6,449,486* Issued to *Polaris Wireless Inc.*, May 1999.

- [Rap02] T.S. Rappaport, *Wireless Communications: Principles and Practice*, Prentice-Hall Inc., New Jersey, 2nd edition, 2002.
- [Sak92] S. Sakagami, S. Aoyama, K. Kuboi, S. Shirota, and A. Akeyama, "Vehicle Position Estimates by Multibeam Antennas in Multipath Environments," *IEEE Transactions on Vehicular Technology*, vol. **41**, no. 1, pp. 63 – 68, Feb 1992.
- [Wei03] A.J. Weiss, "On The Accuracy of A Cellular Location System Based on RSS Measurements," *IEEE Transactions on Vehicular Technology*, vol. **52**, no. 6, pp. 1508 – 1518, Nov 2003.
- [Zha02] Yilin Zhao, "Standardization of Mobile Phone Positioning for 3G Systems," *IEEE Communications Magazine*, vol. **40**, no. 7, pp. 108–116, July 2002.